

Major Miocene exhumation by fault-propagation folding within a metamorphosed, early Paleozoic thrust belt: Northwestern Argentina

D. M. Pearson,^{1,2} P. Kapp,¹ P. W. Reiners,¹ G. E. Gehrels,¹ M. N. Ducea,^{1,3} A. Pullen,^{1,4} J. E. Otamendi,⁵ and R. N. Alonso⁶

Received 7 October 2011; revised 2 May 2012; accepted 27 June 2012; published 17 August 2012.

[1] The central Andean retroarc thrust belt is characterized by a southward transition at $\sim 22^\circ\text{S}$ in structural style (thin-skinned in Bolivia, thick-skinned in Argentina) and apparent magnitude of Cenozoic shortening (>100 km more in the north). With the aim of evaluating the abruptness and cause of this transition, we conducted a geological and geo-thermochronological study of the Cachi Range ($\sim 24\text{--}25^\circ\text{S}$), which is a prominent topographic feature at this latitude. Our U-Pb detrital zircon results from the oldest exposed rocks (Puncoviscana Formation) constrain deposition to mainly Cambrian time, followed by major, Cambro-Ordovician shortening and ~ 484 Ma magmatism. Later, Cretaceous rift faults were locally inverted during Cenozoic shortening. Coupled with previous work, our new (U-Th)/He zircon results require 8–10 km of Miocene exhumation that was likely associated with fault-propagation folding within the Cachi Range. After Miocene shortening, displacement on sinistral strike-slip faults demonstrates a change in stress state to a non-vertically oriented σ_3 . This change in stress state may result from an increase in gravitational potential energy in response to significant crustal thickening and/or lithospheric root removal. Our finding of localized Cenozoic shortening in the Cachi Range increases the estimate of the local magnitude of shortening, but still suggests that significantly less shortening was accommodated south of the thin-skinned Bolivian fold-thrust belt. Our results also underscore the importance of the pre-existing stratigraphic and structural architecture in orogens in influencing the style of subsequent deformation.

Citation: Pearson, D. M., P. Kapp, P. W. Reiners, G. E. Gehrels, M. N. Ducea, A. Pullen, J. E. Otamendi, and R. N. Alonso (2012), Major Miocene exhumation by fault-propagation folding within a metamorphosed, early Paleozoic thrust belt: Northwestern Argentina, *Tectonics*, 31, TC4023, doi:10.1029/2011TC003043.

1. Introduction

[2] Subduction of the Farallon and Nazca oceanic plates beneath the western margin of South America is regarded as a Cenozoic archetype of a contractional ocean-continent convergent margin system. As such, determining the style, timing, and kinematics of deformation in the Andes are

crucial for understanding how Cordilleran-style orogens evolve and the extent to which their evolution is modulated by geodynamic and climatic processes, and other factors like pre-existing heterogeneity in crustal architecture [e.g., *Allmendinger and Gubbels*, 1996; *Strecker et al.*, 2007; *DeCelles et al.*, 2009]. A significant amount of research in the central Andes has focused on thin-skinned shortening within the thick (~ 14 km [*Egenhoff*, 2007]) Paleozoic package of sedimentary rocks in the retroarc thrust belt of northernmost Argentina and Bolivia north of $\sim 22^\circ\text{S}$ [e.g., *Sheffels*, 1990; *Baby et al.*, 1997; *McQuarrie*, 2002]. Southwest of Salta, Argentina (Figure 1), however, despite a similar subduction configuration to its Bolivian and northernmost Argentine counterpart (e.g., similar age of the subducting oceanic Nazca plate and relative convergence velocity [*Pardo-Casas and Molnar*, 1987]), it is thought that steeply dipping, thick-skinned and locally inverted reverse faults accommodated significantly less shortening [e.g., *Allmendinger et al.*, 1983; *Grier et al.*, 1991]. Although the large gradient in along-strike shortening magnitude (>100 km) and style have been previously recognized [e.g., *Isacks*, 1988; *Kley and Monaldi*, 1998], few structural studies have evaluated existing

¹Department of Geosciences, University of Arizona, Tucson, Arizona, USA.

²Now at Department of Geosciences, Idaho State University, Pocatello, Idaho, USA.

³Facultatea de Geologie Geofizica, University of Bucharest, Bucharest, Romania.

⁴Now at Department of Earth and Environmental Sciences, University of Rochester, Rochester, New York, USA.

⁵Departamento de Geología, Universidad Nacional de Río Cuarto, Río Cuarto, Argentina.

⁶Departamento de Geología, Universidad Nacional de Salta, Salta, Argentina.

Corresponding author: D. M. Pearson, Department of Geosciences, Idaho State University, 921 S. 8th Ave., Pocatello, ID 83209, USA. (pearsond@email.arizona.edu)

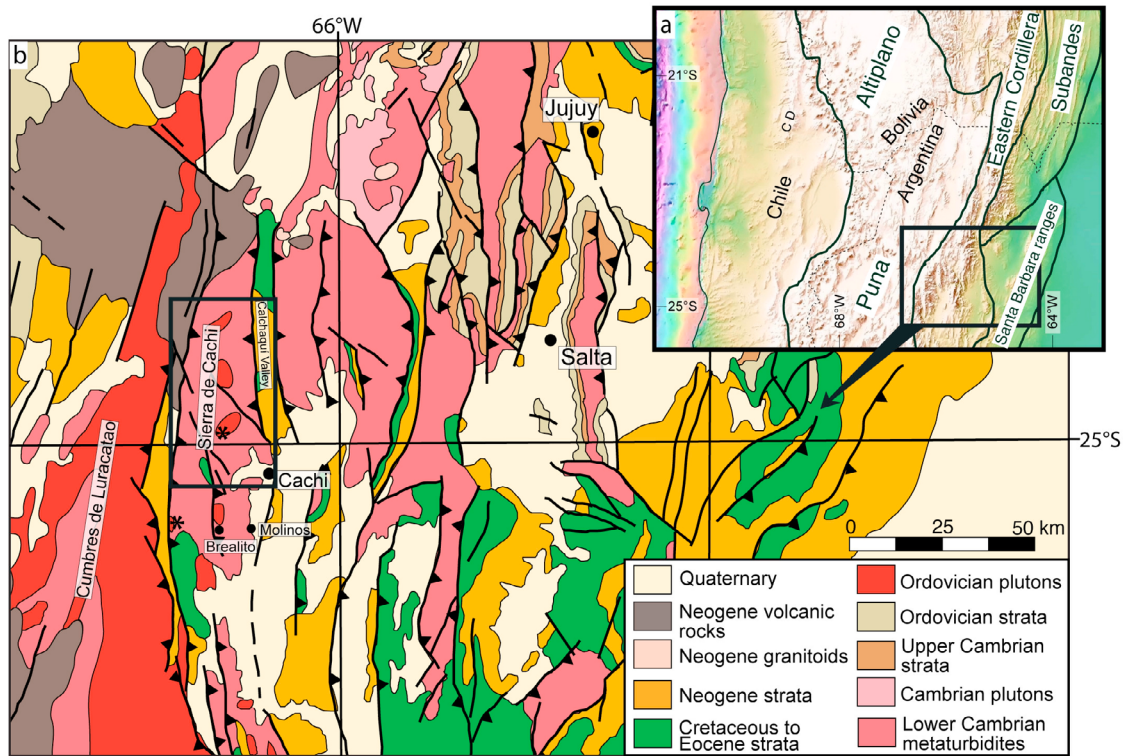


Figure 1. (a) Shaded relief map showing orogen-scale tectonomorphic subdivisions and general geography. CD – Cordillera de Domeyko. (b) Regional geological map of the study area in northwestern Argentina after *Salfity and Monaldi* [2006]. *Approximate locations of apatite fission track samples from *Deeken et al.* [2006] referred to in this study.

estimates of the shortening magnitude accommodated within the Argentine retroarc thrust belt at the latitude of this transition, particularly within the cores of high-elevation mountain ranges in northwestern Argentina where the majority of Cenozoic deformation was likely accommodated.

[3] This paper focuses on the high-elevation (up to 6,380 m) Cachi Range within the Eastern Cordillera tectonomorphic province of the Andean retroarc thrust belt of northwestern Argentina (Figure 1). We document the age, style, and history of deformation of rocks in the Cachi Range using geological mapping and structural analysis coupled with geo- and thermo-chronology. Our results: (1) revise and further our understanding of the lower Paleozoic framework upon which the modern central Andes were formed; (2) confirm a small magnitude of shortening on discrete faults but underscore the likelihood of a larger, but moderate magnitude of shortening by fault-propagation folding; and (3) illuminate a regional-scale change in stress state in northwestern Argentina during late Neogene time. Furthermore, our results are consistent with previous work in the region that underscore the first-order importance of the pre-existing structural and stratigraphic framework in controlling spatial variations in the style and magnitude of crustal deformation [e.g., *Grier et al.*, 1991; *Allmendinger and Gubbels*, 1996; *Kley et al.*, 1999].

2. Regional Geological Background

[4] Tectonomorphic provinces of the central Andean retroarc in northwestern Argentina include, from west to east (Figure 1a): 1) the Puna plateau, a relatively low relief,

topographically high (average elevation ~ 4500 m) region of internal drainage, where older thrust belt structures are mostly buried by Cenozoic sedimentary and volcanic rocks; 2) the Eastern Cordillera, a high relief, topographically high (peak elevations >6000 m), externally drained Cenozoic thrust belt with predominantly west-vergent structures; and 3) the Santa Bárbara Ranges, a region near the modern deformation front that consists of mainly east-dipping reverse faults. In contrast to the Andean thrust belt in Bolivia, pre-Cenozoic tectonics imparted a crustal structure that strongly influenced and complicates our ability to resolve the style and kinematic history of Andean deformation in northwestern Argentina. For example, not exposed in Bolivia but widespread in northwestern Argentina are Neoproterozoic to Cambrian deep-marine sedimentary rocks of the Puncoviscana Formation and igneous and high-grade metamorphic rocks related to early Paleozoic terrane consolidation. Additionally, continental rifting in Cretaceous time that affected most of northwestern Argentina created structures favorable to inversion during Andean orogenesis [*Kley et al.*, 1999]. The protracted, multistage history of sedimentation, magmatism, metamorphism, and deformation near the Cachi Range is summarized in Figure 2.

2.1. Puncoviscana Formation and Paleozoic Tectonics

[5] Tectonic processes that affected the west-central margin of South America began in the Neoproterozoic, when a package of turbidites (the >2000 -m-thick Puncoviscana Formation) were deposited in northern and central Argentina in a region >1000 km north-south by 250 km east-west in


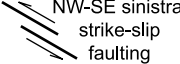



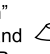
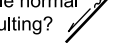


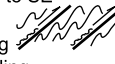
Time	Regional Stratigraphy	Magmatism/ Metamorphism	Deformation
Quaternary		Mafic magmatism 	NW-SE sinistral strike-slip faulting 
Neogene			W verging, E-W shortening 
Paleogene	Quebrada de los Colorados Formation Santa Bárbara Subgroup Balbuena Subgroup		
Cretaceous	Pirgua Subgroup	Local, extension-related mafic magmatism 	Rifting 
Ordovician	Santa Victoria Group Mesón Group	"Famatinian" magmatism and high T, low P metamorphism 	Ductile normal faulting?  Major E verging thrusting 
Cambrian	Puncoviscana Formation	"Pampean" magmatism 	Major E to SE verging thrusting and folding 
Neo-proterozoic			

Figure 2. Tectonostratigraphic chart representative of the Eastern Cordillera at the latitude of the Cachi Range. Time correlations are based upon *Ogg et al.* [2008].

extent [e.g., *Turner, 1960; Jezek et al., 1985; Aceñolaza et al., 1988*]. The tectonic setting of the Puncoviscana basin is debated, but most authors argue for a passive margin setting [*Jezek et al., 1985; Aceñolaza et al., 1988; Rapela et al., 1998; Piñán-Llamas and Simpson, 2006; Adams et al., 2008*]. Recent U-Pb detrital zircon results from the Puncoviscana Formation are compatible with a passive margin setting in the Neoproterozoic and indicate that deposition continued during <555 Ma "Pampean" magmatism [*Adams et al., 2008, 2011*], which signaled the beginning of subduction throughout the region and was coeval with an episode of up to 50% crustal shortening in northwestern Argentina [*Rapela et al., 1998; Piñán-Llamas and Simpson, 2006; Schwartz et al., 2008*]. Metamorphic ages indicate that deformation took place during Neoproterozoic to Early Cambrian time and authors have proposed that major shortening ceased by 530–520 Ma, based upon the presence of relatively undeformed Cambrian plutons that intruded the strongly folded Puncoviscana Formation [*Piñán-Llamas and Simpson, 2006, and references therein*]. At ~500 Ma, Upper Cambrian shallow marine platform

deposits of the Mesón Group were deposited upon a regional angular unconformity (the "Tilcaric" unconformity) that postdates the folded Puncoviscana Formation, presumably constraining the end of the "Pampean cycle" to 510–500 Ma [*Adams et al., 2011*].

[6] At 490–485 Ma, subduction was reestablished along the margin with concomitant, "Famatinian" continental arc magmatism and regional low-pressure, high-temperature metamorphism [*Rapela et al., 1998; Büttner et al., 2005; Otamendi et al., 2010*]. Ordovician plutons and volcanic rocks on the Puna, west of the Cachi Range, represent the upper-crustal levels of the magmatic arc system [*Coira et al., 1982*]; deeper equivalents (20–25 km paleodepths) of this arc are exposed toward the south [*Otamendi et al., 2008*]. Ordovician arc magmatism ended at ~465 Ma in most of Argentina with the accretion of the Precordillera terrane during "Ocoyoc" orogenesis [e.g., *Rapela et al., 1998; Ducea et al., 2010*], with major shortening accommodated by N-S striking, W-dipping thrust faults [e.g., *Astini and Dávila, 2004*]. North of the accreted Precordillera terrane (<28°S modern latitude), an extensive back-arc basin developed.

These Cambro-Ordovician orogenic events strongly controlled regional patterns of mid to late Paleozoic deposition and yielded a crust exposed at different along-strike structural levels. Intermittent magmatism and sedimentation from Late Silurian to Cretaceous time occurred along the South American plate margin, but orogenesis of this age is not well documented within northwestern Argentina.

2.2. Cretaceous Rifting

[7] Cretaceous continental rifting affected much of northwestern Argentina, southern Paraguay, Bolivia, and northeastern Chile [Salfity and Marquillas, 1994]. Up to 5.5 km of sediment, the Salta Group, were deposited in concomitant basins [Salfity and Marquillas, 1994; Monaldi et al., 2008]. Rift basin fill includes non-marine conglomerate and sandstone of the Pirgua Subgroup [Salfity and Marquillas, 1994; Kley and Monaldi, 2002]. Overlying these conglomerates and superjacent structural highs is a thinner but more regionally contiguous package of post-rift Upper Cretaceous to lower Eocene sandstone, limestone, and shale of the Balbuena and Santa Bárbara Subgroups [Salfity and Marquillas, 1994; Kley and Monaldi, 2002]. Normal faults associated with the Salta rift generally strike ~ENE, N-S, and NW, have moderate to steep dips, and accommodated <10% extension [e.g., Grier et al., 1991; Kley and Monaldi, 2002; Masafiero et al., 2003; Monaldi et al., 2008].

[8] Modern high-elevation exposures of marine-influenced limestones of the Balbuena Subgroup in the Argentine Eastern Cordillera and Puna plateau require the development of major topographic and structural relief during Cenozoic time. In addition, Cretaceous strata were deposited unconformably upon the Puncoviscana Formation at this latitude, demonstrating that thick overlying Paleozoic strata present in southern Bolivia were not deposited or were eroded in northern Argentina prior to Andean orogenesis [Salfity and Marquillas, 1994]. Cretaceous rift structures were widely inverted during Andean orogenesis, identified by Cenozoic reverse fault hanging walls that correspond spatially to syn-rift depocenters [e.g., Grier et al., 1991; Cristallini et al., 1997; Kley and Monaldi, 2002; Masafiero et al., 2003; Carrera et al., 2006; Monaldi et al., 2008].

2.3. Cenozoic Thrust Belt Evolution

[9] Plutons whose ages span much of Phanerozoic time suggest that subduction occurred somewhat continuously beneath the western margin of South America since Cambrian time, but the modern expression of the Andes was apparently only attained during major Cenozoic shortening in the central Andes [e.g., Coney and Evenchick, 1994]. Balanced cross sections and the distribution of the high-elevation Andes suggest that the magnitude of Cenozoic retroarc shortening in the central Andes varies along strike, reaching a maximum value within the Bolivian orocline and decreasing to the north and south [Isacks, 1988; Kley and Monaldi, 1998]. In northern Argentina, <70 km of upper-crustal shortening was estimated in the region [e.g., Grier et al., 1991], which is ~160 km less than that predicted if the high elevation Puna and Eastern Cordillera are isostatically compensated by a tectonically thickened crust [Isacks, 1988; Kley and Monaldi, 1998]. Shortening was accommodated by different structural styles along strike (thin-skinned

shortening to the north and basement-involved shortening to the south [Allmendinger and Gubbels, 1996; Kley et al., 1999]), but it is unclear if this along-strike change is abrupt or gradational and why, geodynamically, there is such a large along-strike variation, given that the subduction configuration does not change drastically.

[10] The retroarc thrust belt in northwestern Argentina and Bolivia was not a steadily eastward-propagating system, but instead was characterized by periods of rapid foreland-ward propagation [e.g., Coutand et al., 2001; McQuarrie, 2002; Oncken et al., 2006; Barnes et al., 2008]. In Bolivia, at ~19°S, the thrust front generally propagated eastward through time but during the Eocene, deformation appears to have jumped from the Cordillera de Domeyko in the modern forearc (Figure 1a) >300 km to the east to the Eastern Cordillera, with subsequent shortening propagating eastward mainly in the Miocene [e.g., McQuarrie, 2002; Oncken et al., 2006; Barnes et al., 2008].

[11] Deformation in northern Argentina appears to have also been active in the Eastern Cordillera by late Eocene time [e.g., Coutand et al., 2001; Carrapa and DeCelles, 2008] and is documented by growth strata near the Cachi Range [Hongn et al., 2007; Bosio et al., 2009]. However, the main period of exhumation along the eastern edge of the Puna plateau did not occur until ~20 Ma, the age of apatite fission track (AFT) samples collected from granitoids in the Cumbres de Luracatao (Figure 1b) [Deeken et al., 2006]. Two additional AFT samples collected from the Cachi Range, one ~15 km south of our study area from the hanging wall of the E-dipping Cachi fault (Figures 1b and 3) and one from the core of the range in the hanging wall of the Las Cuevas fault (Figures 1b and 3), also yielded mid-Miocene ages (~15 Ma [Deeken et al., 2006]), hinting at a progressive eastward propagation of deformation.

2.4. Transition From Thrusting to Strike-Slip Faulting

[12] Active deformation in the Puna plateau and flanking Eastern Cordillera is characterized by normal and strike-slip faulting, demonstrating that an important change in the state of stress occurred after Neogene thrusting in the region, at some time between the late Miocene and Quaternary [Allmendinger et al., 1989; Marrett et al., 1994; Schoenbohm and Strecker, 2009]. At ~27°S, Schoenbohm and Strecker [2009] proposed that lithospheric delamination and associated gravitational collapse in the southern Puna [Kay et al., 1994] caused the transition to normal faulting. DeCelles et al. [2009] suggested that lithospheric delamination events could be expected to elicit an orogenic response in the retroarc thrust belt by inducing isostatic rebound and topographic uplift above the delamination and imposition of supercritical orogenic wedge taper, promoting foreland-ward deformation propagation.

[13] Geophysical observations corroborate the notion that lithosphere has been removed from beneath the Puna plateau, west of the Cachi Range. Crustal thickness reaches ~65 km thick beneath the Altiplano [Beck and Zandt, 2002]. In contrast, the depth to the Moho beneath the topographically higher Puna plateau at ~25°S is 42–48 km [e.g., Yuan et al., 2002]. Beneath this thinner crust at 100–200 km depth, is a region inferred to comprise relatively cold lithosphere; coupled with volcanic rock geochemistry [Kay et al.,

1994], this region was interpreted as recently delaminated mantle lithosphere [Schurr *et al.*, 2006].

3. Geology of the Cachi Range

3.1. Fieldwork

[14] We conducted geological mapping and structural analysis along several foot traverses in the Cachi Range (Figure 1), concomitant with sample collection for U-Pb and (U-Th)/He analysis of detrital and igneous zircons, and petrography.

3.2. Rock Units

[15] The Cachi Range is cored by variably metamorphosed argillite, siltstone, and lesser coarse-grained turbiditic sandstone of the Puncoviscana (lower metamorphic grade) and La Paya (higher metamorphic grade) Formations (Figures 3–7) [Galliski, 1983; Omarini *et al.*, 1999; Hongn and Seggiaro, 2001]; these rocks have mainly Neoproterozoic to Cambrian protoliths. In most places, the La Paya Formation exhibits a gradational contact with the Puncoviscana Formation; for this reason and for simplicity, we refer to them collectively as the Puncoviscana Formation. Northeast of the Cachi Range, Cambrian plutons (536–513 Ma U-Pb zircon ages [Adams *et al.*, 2011, and references therein]) intruded the Puncoviscana Formation. West of the Cachi Range, the Cumbres de Luracatao mainly expose gneisses and Ordovician granitoids and represent the northernmost locality where a significant volume of Famatinian magmatic rocks are exposed.

[16] In the central part of the Cachi Range, a small volume of Ordovician granitoids intruded the Puncoviscana Formation (Figure 3) [Galliski, 1983; Hongn and Seggiaro, 2001; Méndez *et al.*, 2006]. These Ordovician igneous rocks are of three types: 1) two-mica bearing granitoids; 2) pegmatites that are in many places associated with the two-mica bearing granitoids; and 3) porphyritic (0.5–1 cm square plagioclase), biotite- and epidote-bearing tonalites.

[17] The southern part of the map area (Figures 3 and 7) exposes the unconformable relationship between syn-rift Cretaceous rocks of the Pirgua Subgroup and deformed Puncoviscana Formation and Ordovician granitoids. The lower part of the Pirgua Subgroup in the Cachi Range consists of coarse-grained, clast-supported breccias that fine upward into locally derived sandstones. To the south, in the Brealito area (Figure 1b), the Pirgua Subgroup reaches a thickness of 3000 m [Carrera *et al.*, 2006]. No Paleogene or Neogene rocks are exposed in the Cachi Range. However, west of the range in the Luracatao Valley, ~1 km of Paleocene to Eocene fluvial sandstones and paleosols of the Santa Bárbara Subgroup and Eocene fluvial conglomerates, sandstones, siltstones, and mudstones of the overlying Quebrada de los Colorados Formation are exposed [Bosio *et al.*, 2009]. East of the Cachi Range, in the Calchaquí Valley (Figures 3

and 5), Upper Cretaceous carbonates and sandstones of the Yacoraite Formation are overlain by sandstones and paleosols of the Paleogene Santa Bárbara Subgroup, which is in turn overlain by an Eocene to Oligo-Miocene succession of rocks of the Quebrada de los Colorados Formation, totaling ~2 km in thickness [Hongn *et al.*, 2007]. These Late Cretaceous to Cenozoic rocks exposed along the range margins are consolidated into one map unit in this study.

[18] Shoshonites of likely Quaternary age unconformably overlie these rocks near the eastern range margin and in the core of the northern part of the Cachi Range (Figures 3 and 5). In the higher elevation parts of the range, glacial deposits and landslides of likely late Pleistocene age are abundant. Dark alluvial and landslide deposits, also of likely Pleistocene age [Trauth *et al.*, 2000], unconformably blanket Cenozoic rocks and range-bounding reverse faults in many places at the range margins, especially in the northeast. Additional Quaternary terrace deposits, in turn, overlie these sediments (mapped as “older alluvium” here), and are locally covered by Holocene alluvium.

3.3. Penetrative Deformation and Metamorphism

[19] Bedding-parallel cleavage and foliations within the Puncoviscana Formation in the Cachi Range generally dip moderately to steeply to the northwest; folds within the Puncoviscana typically plunge moderately to shallowly to the southwest (see stereograms in Figure 3). Northwest of La Poma, the Puncoviscana Formation is tightly folded and transposed (Figure 4a) and cleavages/foliations are NE-striking and generally moderately to steeply NW-dipping. Petrographic observations of the fine-grained metamorphic assemblages indicate that, in addition to quartz, biotite is common as a fine-grained, primary-cleavage/foliation-forming matrix phase. Coarser biotite also pseudomorphed the rims of diamond-shaped porphyroblasts of uncertain mineralogy. Primary muscovite and chlorite are rare; more commonly, they grew as irregularly oriented retrograde phases. Anhydrous cordierite is also present locally, and increases in size toward the core of the range.

[20] To the south, at the latitude of Cachi, low-grade, generally slaty and phyllitic rocks on the eastern margin of the range are also transposed, with rootless, isoclinal folds and open to tight chevron folds with variably oriented axes (Figure 4b). These rocks display a gradational contact with high-grade rocks in the core of the range. At this latitude, rocks at the range margins petrographically resemble those observed to the north, but contain larger cordierite porphyroblasts and rare chloritoid oriented obliquely to matrix biotite. Toward the core of the range, foliations within and near Ordovician granitoids strike more consistently to the N-S (Figures 3 and 7) and grade into schists that locally exhibit crenulation cleavages and well-defined stretching lineations. Farther westward, rocks transition to steeply dipping (65–90°W), high-grade, anatectic gneisses, with

Figure 3. Geological map of the Cachi Range showing major structural and lithological features. Location of map is shown in Figure 1b. Inset stereograms are equal-area lower-hemisphere projections. We were unable to discern differences among the orientations of bedding, bedding parallel cleavages, primary cleavages, and foliations in Cambrian metaturbidites away from Ordovician granitoids; given the multiphase deformational history of these rocks, we group these data in the lower stereogram to demonstrate their high variability, but overall consistency with measured NE-trending fold axes.

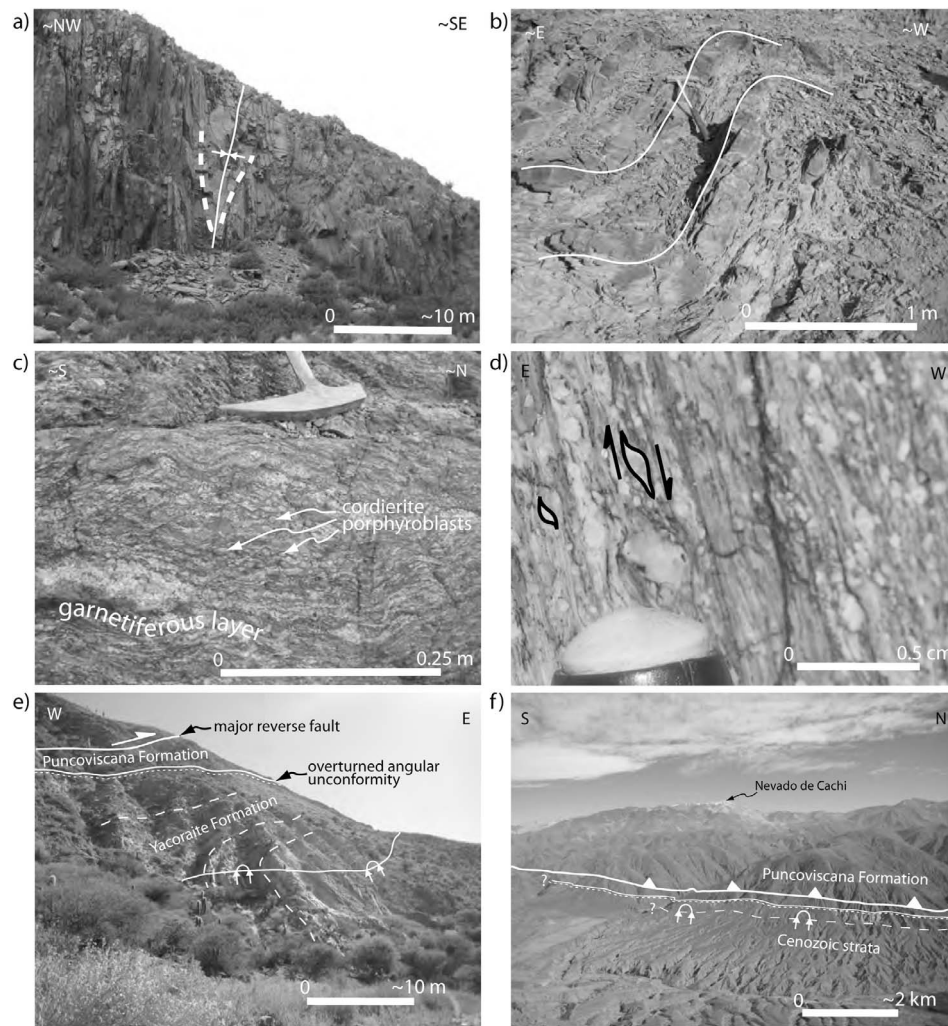


Figure 4. (a) View toward northeast of tight, NE-plunging chevron fold in the Puncoviscana Formation in the northern part of the Cachi Range, west of La Poma. (b) View toward south of variably oriented open chevron folds in relatively low-grade rocks at the eastern range margin near the town of Cachi. (c) View toward west of cordierite- and garnet-bearing gneiss, exposed in the highest grade core of the range, near Ordovician granitoids, and in the hanging wall of the Las Cuevas fault at $\sim 25.1^{\circ}$ S latitude. (d) View toward south of sigma-type porphyroclasts in ultramylonitic orthogneiss indicating likely Ordovician, normal-sense displacement. (e) Oblique view toward north of Yacoraite Formation carbonates folded into an overturned syncline in footwall of the major E-verging, range-bounding reverse fault (Toro Muerto fault). The reverse fault is located within the Puncoviscana Formation and overturned the angular unconformity upon which the Yacoraite Formation was deposited. (f) View toward west of the Cachi Range, from east of La Poma, showing the Toro Muerto fault within the Puncoviscana Formation and Cenozoic strata forming a locally overturned footwall syncline.

ptygmatic folds, interfingered sills, and no apparent relict sedimentary features. These gneisses are interspersed with Ordovician granitoids, reached granulite facies-equivalent metamorphic conditions, and underwent anatexis; metamorphic phases include potassium feldspar, retrograded cordierite (<1 mm to 1.5 cm in diameter), rare garnet, and biotite (Figure 4c). A fault contact (described in the next section) at the western margin of these high-grade rocks separates them from moderately to steeply W- to NW-dipping lower grade phyllites to the west, which have occasional concordantly oriented metamorphosed silicic volcanic rocks or sills. Here,

Ordovician granitoids are generally absent, although they are exposed to the southwest of Brealito (Figure 1b).

4. Structural Geology

[21] Faults in the Cachi Range reflect at least three episodes of deformation. From older to younger, these are:

[22] 1) N-S striking, W-dipping ductile shear zones that mainly accommodated E-W shortening. These faults are approximately parallel to the regional fabric exhibited by Puncoviscana Formation in the core of the range, appear to

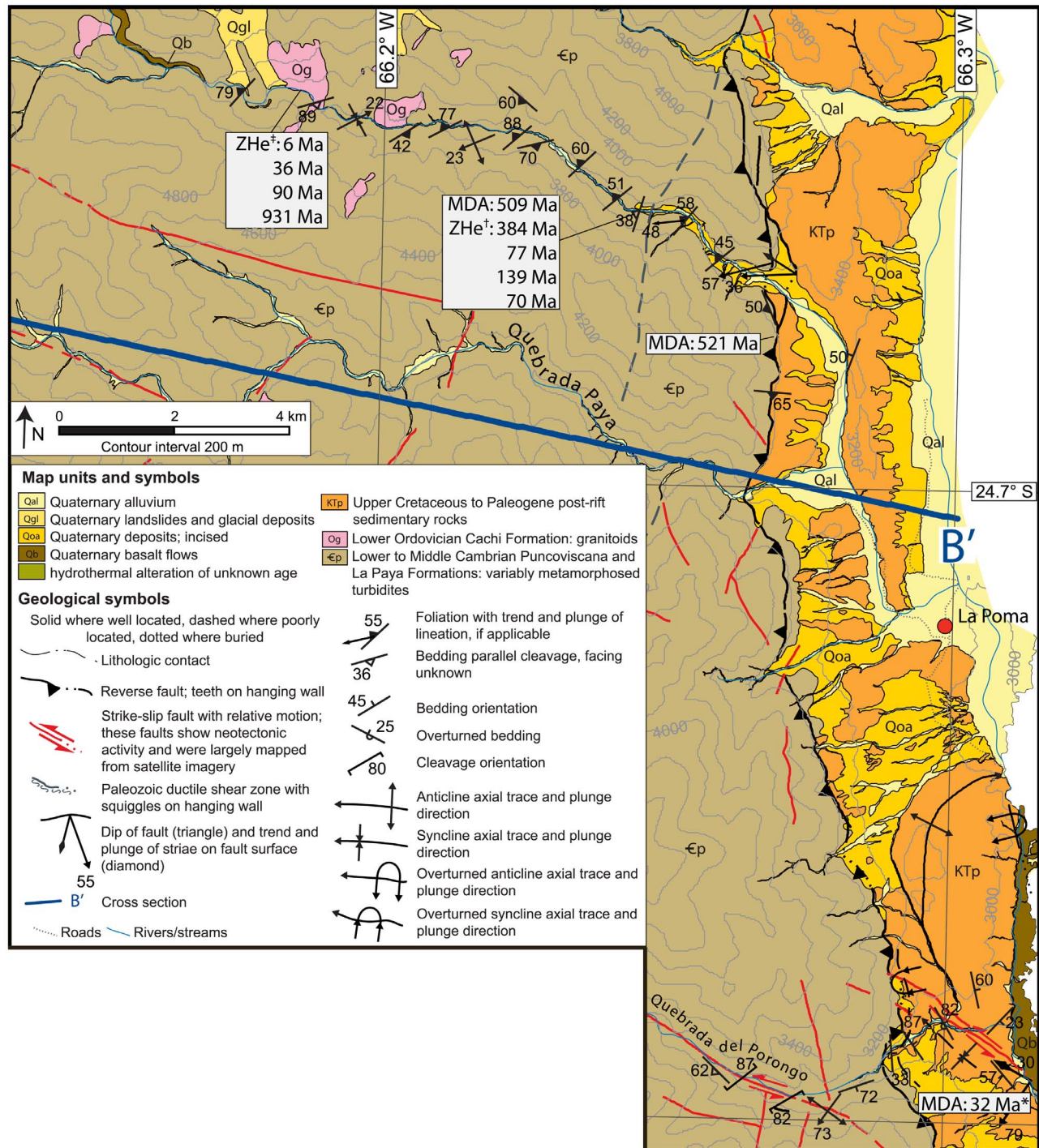


Figure 5. Geological map of northeastern margin of the Cachi Range near La Poma. See Figure 3 for location. Age-dating abbreviations – MDA: maximum depositional age from detrital zircon results; ZHe: (U-Th)/He zircon. *This detrital zircon sample only yielded one Cenozoic zircon, which results in a statistically insignificant MDA. †Sample did not yield a single population of ages with respect to (U-Th)/He zircon, implying exhumation was <8–9 km. ‡Sample yielded (U-Th)/He zircon ages that are strongly correlated with effective uranium concentrations, suggesting that (U-Th)/He zircon results from this sample are compromised by radiation damage in zircon.

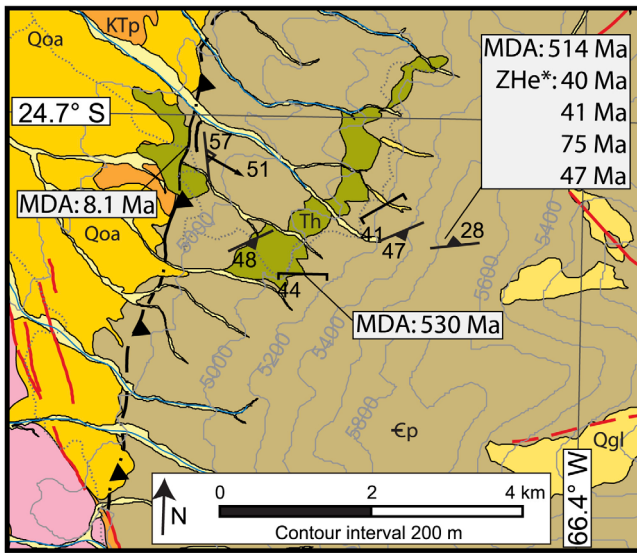


Figure 6. Geological map of northwestern margin of the Cachi Range, west of La Poma. See Figure 3 for location. Map symbols are the same as Figure 5. Age-dating abbreviations – MDA: maximum depositional age from detrital zircon results; ZHe: (U-Th)/He zircon. *Sample did not yield a single population of ages with respect to (U-Th)/He zircon, implying exhumation was <8–9 km.

bear no relation to the modern range topographic expression, and do not cut rocks younger than Cambro-Ordovician in age. [23] 2) N-S striking, mainly E-dipping brittle reverse faults that locally modified older fabrics. These faults are expressed

in the modern topography, juxtaposed rocks of markedly different grade and age, and locally expose Cretaceous syn-rift deposits in their hanging walls (and therefore are probably reactivated normal faults).

[24] 3) Mainly NW-striking, generally NE-dipping sinistral faults with minimal dip-slip displacement that are discontinuous and often en-echelon. These near-vertical faults have locally reactivated older faults described above, form prominent lineaments on aerial imagery, and likely have been active in the Quaternary.

4.1. Paleozoic Structures

[25] The monotonous nature and lack of a tectonostratigraphic framework for the Puncoviscana Formation makes field identification of Paleozoic faults and shear zones difficult. However, significant ductile structures with well-preserved strain fabrics were investigated in the field. One structure, observed ~6 km directly west of Cachi, is a 55–60°W-dipping, protomylonitic shear zone within phylitic rocks of the Puncoviscana Formation (Figures 3 and 7). Field observations and petrographic thin sections reveal a well-developed stretching lineation, S-C fabrics, and occasional delta clasts that consistently suggest a top-to-the-east sense of displacement. An additional ductile structure, ~13 km west of Cachi, is exposed within a package of steeply dipping (~85°W) ortho- and paragneisses (Figure 7). This shear zone is an ultramylonitic shear zone with abundant plagioclase sigma porphyroclasts, which, along with strongly developed stretching lineations and S-C fabrics, consistently display a top-to-the-west (normal sense) displacement (Figure 4d). Petrographic observations indicate that this rock is an orthogneiss; based upon U-Pb age dating

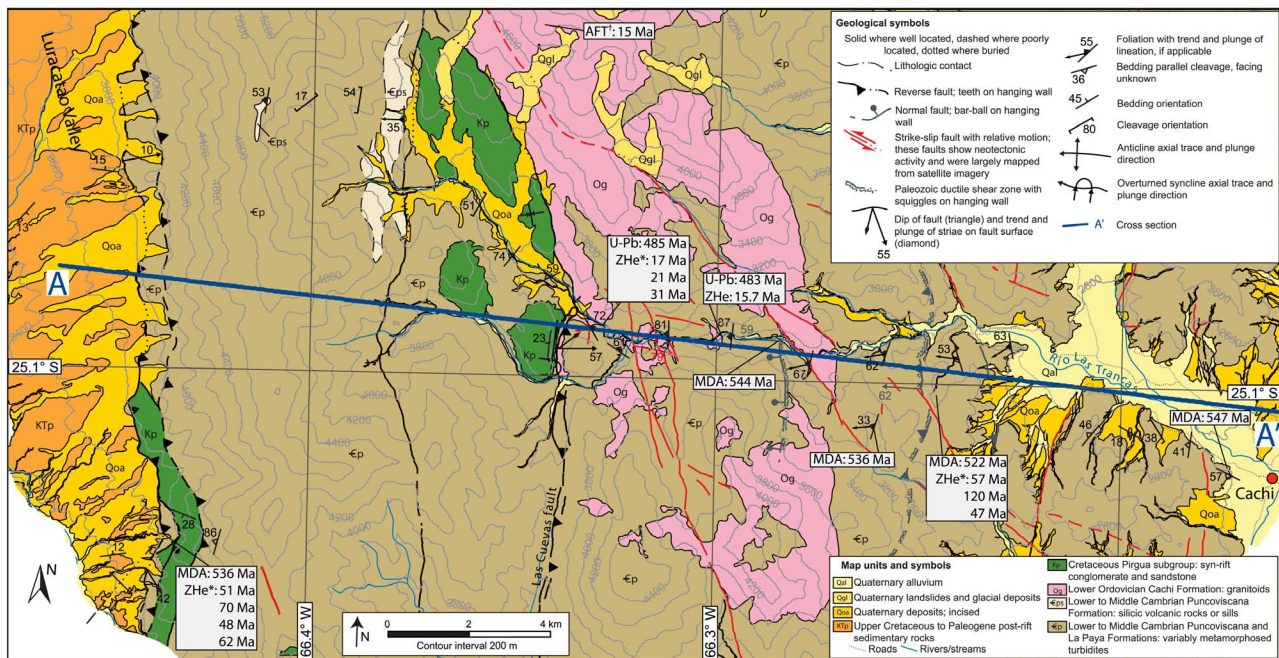


Figure 7. Geological map of the south-central part of the Cachi Range between Cachi and Luracatao. See Figure 3 for location. Age-dating abbreviations – MDA: maximum depositional age from detrital zircon results; U-Pb: U-Pb zircon; ZHe: (U-Th)/He zircon; AFT: apatite fission track. *Sample did not yield a single population of ages with respect to (U-Th)/He zircon, implying exhumation was <8–9 km. †Deeken et al. [2006].

of other granitoids within the range (presented later in Section 5.3.2), we infer that the protolith of this rock is Ordovician in age. Also present is a N-NW striking chloritized zone of mylonitized granitoid with strain fabrics showing an ambiguous sense-of-shear. This may be a Paleozoic fault that was reactivated during late Cenozoic brittle deformation.

[26] Based on our field observations and analysis of aerial photos and satellite imagery, the structurally highest rocks in the core of the range were thrust upon rocks to the east along several west-dipping thrust faults/shear zones. This interpretation of structural duplication of strata is further supported by our U-Pb detrital zircon studies of Puncoviscana Formation rocks described later in this paper. These W-dipping shear zones appear to have overprinted the earlier, generally NE-SW oriented fabrics and are generally concordant with N-S striking fabrics observed near Ordovician granitoids (Figure 3).

4.2. Cenozoic Reverse Faults

[27] North of Palermo Oeste (Figures 3–6), the Cachi Range is flanked on the west and east by oppositely verging reverse faults (Cachi fault and Toro Muerto fault, respectively) that juxtapose the Puncoviscana Formation against the Quebrada de los Colorados Formation and Santa Bárbara and Balbuena Subgroups (Figures 5 and 6). In contrast, at the latitude of Cachi, the eastern range margin appears to not be fault-bounded (Figure 7). Instead, two prominent W-vergent structures, one on the western range margin, the Cachi fault, and one in the range core, the Las Cuevas fault, accommodated uplift of the range. Both of these reverse faults juxtapose Puncoviscana rocks against Mesozoic and Cenozoic sedimentary rocks. The highest grade metamorphic rocks (high-temperature, low-pressure metamorphism as a result of Ordovician orogenesis) were exhumed in the proximal hanging wall of the Las Cuevas fault. Pirgua Group conglomerates are exposed in the footwall of the E-dipping Las Cuevas fault and in the hanging wall of the Cachi fault to the west (Figure 7). The Cachi fault (Figure 3) offsets Quaternary alluvial units ~10 km south of Brealito, and Pleistocene activity has been inferred [Hongn and Seggiaro, 2001]. South of that location, along-strike of the Cachi fault, the Cretaceous Pirgua Subgroup is in fault contact above Ordovician granitoids [Hongn and Seggiaro, 2001]. Pirgua conglomerates reach a maximum thickness adjacent to their western fault boundary [Carrera et al., 2006] and are absent to the west. These observations indicate that the Cachi fault was originally a normal fault at the western boundary of the Salta Rift [Carrera et al., 2006] and was reactivated as a Neogene reverse fault.

[28] Major N-S striking, brittle reverse faults are characterized by blue-gray, up to 200 m wide zones of intense fracturing, with rare throughgoing fault surfaces and rare fault gouge. Abundant cleavages in the fine-grained rocks of the Puncoviscana Formation likely resulted from several episodes of orogenesis, making it difficult to assign penetrative deformation fabrics to specific periods of deformation. We therefore placed more emphasis on folded Mesozoic and Cenozoic footwall rocks with S- to SSE-trending axial traces (Figure 3 stereograms). South of La Poma, an overturned anticline-syncline fold set with a steeply W-dipping axial surface and no exposed associated

fault accommodated ~30 m of reverse-sense structural relief and is consistent with deformation above a propagating fault tip (Figure 5) [e.g., Williams and Chapman, 1983; Erslev, 1991]. Overturned synclines in these younger rocks are common at the more regional scale in the footwalls of the major reverse faults (Figures 4e, 4f and 5). Near Quebrada del Porongo (southernmost area in Figure 5) and in the footwall of the Las Cuevas fault in the core of the Cachi Range (Figure 7), steep (~45–60°) fault zones with distributed strain and layer-parallel slickensides within Puncoviscana metaturbidites structurally overlie overturned footwall synclines within which the folded angular unconformity between Puncoviscana and overlying Cretaceous and Cenozoic rocks can be identified (Figures 4e and 4f). An important observation is that folding of the Puncoviscana Formation is required to accommodate the observed overturned angular unconformity and regional spatial patterns of the depth of exhumation in the Cachi Range (see later discussion of (U-Th)/He thermochronological results).

[29] On the western flank of the mountain range, a fault-bounded sliver of Cretaceous syn-rift strata is exposed in the hanging wall of the Cachi fault (Figures 3 and 7). Similar relationships in other localities have been suggested to be “shortcut” faults, where thrust reactivation along Cretaceous rift faults was unable to accommodate shortening without rupturing more shallowly dipping structures [e.g., Carrera et al., 2006]. Overall, our field observations of steep fault surfaces and the importance of fault-propagation folding, coupled with regional observations indicating that existing Cretaceous extensional structures were reactivated during Cenozoic time are compatible with a thick-skinned style of deformation.

4.3. Strike-Slip Faults

[30] NW-SE striking faults are abundant in the Cachi Range (Figure 3). They are characterized by prominent lineaments in aerial imagery, parallel many major drainages, are locally topographically expressed in Quaternary terrace deposits (e.g., near Palermo Oeste), and appear to not have accommodated significant vertical displacement. The NW-SE striking fault set separates N-S striking structures in a sinistral sense in several localities near the Cachi Range. This includes at the northwestern margin of the range, where a sinistral fault separates the Cachi fault by up to 7 km and near Palermo Oeste, where the Palermo fault parallels and appears to control the geometry of the NW-SE trending range front (Figure 3). At the outcrop scale, brittle fault fabrics and kinematic indicators, tool marks, and NE-striking, antithetic dextral faults also indicate a sinistral sense of displacement. Abundant regional scale, NW-striking, right stepping, en-echelon lineaments, and apparent antithetic NNE-striking faults are also consistent with a sinistral sense of slip (Figure 3).

5. U-Pb Zircon Geochronology

5.1. Analytical Methods

[31] U-Pb zircon geochronology by laser-ablation inductively coupled-plasma mass-spectrometry (LA-ICP-MS), following methods described by Gehrels et al. [2008], was applied to two igneous and 11 detrital samples to better constrain ages of deposition, magmatism, metamorphism,

Table 1 (Sample). U-Pb (Zircon) Geochronologic Analyses by Laser-Ablation Multicollector ICP Mass Spectrometry^a [The full Table 1 is available in the HTML version of this article]

Sample	U (ppm)	²⁰⁶ Pb*/ ²⁰⁴ Pb	U/Th	²⁰⁶ Pb*/ ²⁰⁷ Pb*	Isotopic Ratios				Apparent Ages (Ma)				Best Age (Ma)	± (Ma)	Conc (%)				
					± (%)	²⁰⁷ Pb*/ ²³⁵ U	± (%)	Error Corr.	²⁰⁶ Pb*/ ²³⁸ U	± (%)	²⁰⁷ Pb*/ ²³⁵ U	± (Ma)				²⁰⁶ Pb*/ ²⁰⁷ Pb*	± (Ma)		
08DP08 ^b																			
Grain																			
2	416	65130	2.5	16.1741	1.0	0.8848	4.4	0.1038	4.3	0.97	636.6	26.1	643.6	21.0	668.1	21.5	636.6	26.1	95
4	322	27825	1.6	17.9589	4.1	0.5736	4.9	0.0747	2.7	0.54	464.5	12.0	460.4	18.2	439.7	91.9	464.5	12.0	106
5	444	39575	1.5	17.0524	1.4	0.6610	3.5	0.0817	3.2	0.91	506.5	15.5	515.2	14.1	553.8	31.0	506.5	15.5	91
7	280	77115	2.3	13.4203	1.2	1.8672	1.8	0.1817	1.4	0.76	1076.5	13.7	1069.5	12.0	1055.4	23.6	1055.4	23.6	102
8	300	27855	6.0	17.5830	2.9	0.6038	3.2	0.0770	1.4	0.43	478.2	6.4	479.6	12.3	486.6	63.8	478.2	6.4	98
10	402	152450	9.2	8.0191	1.0	5.2064	2.5	0.3028	2.3	0.92	1705.2	34.2	1853.7	21.2	2024.6	17.7	2024.6	17.7	84
12	176	17645	1.6	17.2535	7.3	0.6094	7.8	0.0763	2.7	0.35	473.7	12.5	483.2	29.9	528.2	159.9	473.7	12.5	90
13	150	65930	0.8	8.6851	1.7	5.2830	2.7	0.3328	2.2	0.79	1851.8	34.8	1866.1	23.5	1882.1	30.6	1882.1	30.6	98
15	84	23925	1.4	9.8248	1.5	3.4326	1.8	0.2446	1.0	0.55	1410.5	12.7	1511.9	14.2	1656.9	28.0	1656.9	28.0	85
16	305	22760	4.3	16.7698	3.2	0.6264	3.9	0.0762	2.2	0.58	473.3	10.2	493.8	15.2	590.2	68.6	473.3	10.2	80
18	70	21895	3.1	13.3601	2.9	1.8288	5.7	0.1772	4.9	0.86	1051.7	47.6	1055.8	37.4	1064.5	58.3	1064.5	58.3	99
19	265	29605	2.6	17.2167	2.8	0.6438	3.5	0.0804	2.0	0.58	498.4	9.7	504.6	13.9	532.9	62.0	498.4	9.7	94
20	418	31340	8.0	17.0700	2.9	0.6253	3.4	0.0774	1.8	0.52	480.7	8.2	493.2	13.2	551.6	63.1	480.7	8.2	87
22	98	26705	3.0	14.1251	4.1	1.3858	4.9	0.1420	2.7	0.56	855.8	22.0	882.9	29.0	951.5	83.7	855.8	22.0	90
23	102	13075	1.8	17.3732	2.0	0.6587	3.1	0.0830	2.4	0.77	514.0	11.9	513.8	12.6	513.0	44.3	514.0	11.9	100
24	408	42090	21.6	17.8564	4.0	0.5624	4.3	0.0728	1.8	0.41	452.4	7.2	481.9	15.0	452.4	88.2	452.4	7.2	72
25	760	22580	7.9	16.5051	3.5	0.6074	3.9	0.0727	1.7	0.42	453.2	7.7	481.9	15.0	452.4	76.3	452.4	7.7	100
28	350	41270	5.4	8.8855	1.3	3.6714	3.0	0.2366	2.7	0.90	1369.0	32.7	1365.2	23.6	1840.9	23.7	1840.9	23.7	74
30	127	29545	3.3	13.4706	3.7	1.7112	4.7	0.1672	2.9	0.62	996.6	26.9	1012.7	30.3	1047.9	75.0	1047.9	75.0	95
32	381	34030	2.5	16.4573	1.8	0.8409	4.1	0.1004	3.7	0.90	616.6	21.8	619.6	19.2	630.8	39.2	616.6	21.8	98
32	147	16755	0.7	16.8102	4.1	0.6387	4.4	0.0779	1.7	0.38	483.4	7.7	483.4	17.4	585.0	88.2	483.4	7.7	83
33	501	22520	2.6	12.9394	1.6	1.3981	4.3	0.1312	3.9	0.92	794.7	29.5	888.1	25.2	1128.5	32.4	794.7	29.5	70
35	224	25070	1.6	16.8708	2.3	0.6966	2.8	0.0852	1.7	0.59	527.3	8.5	536.8	11.8	577.2	49.4	527.3	8.5	91
38	163	24565	1.8	17.6184	2.6	0.6826	2.8	0.0872	1.0	0.36	539.1	5.2	528.3	11.5	482.2	57.8	539.1	5.2	112
39	118	23520	2.3	13.5582	2.4	1.7154	3.0	0.1687	1.8	0.59	1004.9	16.7	1014.3	19.4	1034.8	49.1	1034.8	49.1	97
42	174	16305	0.8	17.6376	3.1	0.5992	3.6	0.0766	1.8	0.51	476.1	8.4	476.7	13.8	479.8	68.8	476.1	8.4	99
44	56	7590	1.4	16.9981	9.7	0.7223	10.7	0.0890	4.6	0.43	549.9	24.4	552.0	45.8	560.8	211.8	549.9	24.4	98
45	317	37765	1.9	17.0090	2.5	0.6756	3.0	0.0833	1.5	0.52	516.0	7.6	524.1	12.1	559.4	57.0	516.0	7.6	92
46	298	43990	3.6	16.5165	1.7	0.8285	3.0	0.0992	2.5	0.82	610.0	14.5	612.8	13.9	623.1	37.1	610.0	14.5	98
49	207	10665	1.5	12.3957	2.8	1.7630	4.5	0.1585	3.5	0.79	948.4	31.2	1032.0	29.2	1213.5	54.6	1213.5	54.6	78
50	208	20415	3.6	17.6210	2.4	0.6054	2.8	0.0774	1.3	0.48	480.4	6.2	480.6	10.6	481.8	53.6	480.4	6.2	100

^aNotes: (1) All uncertainties are reported at the 1-sigma level, and include only measurement errors. Systematic errors would increase the uncertainty of clusters of ages by 1–2%. (2) U concentration and U/Th are calibrated relative to our Sri Lanka zircon and are accurate to ~20%. (3) Common Pb correction is from ²⁰⁴Pb, with composition interpreted from *Stacey and Kramers* [1975] and uncertainties of 1.5 for ²⁰⁶Pb/²⁰⁴Pb, 0.3 for ²⁰⁷Pb/²⁰⁴Pb, and 2.0 for ²⁰⁸Pb/²⁰⁴Pb. (4) U/Pb and ²⁰⁶Pb/²⁰⁷Pb fractionation is calibrated relative to fragments of a large Sri Lanka zircon of 564 Ma age (2-sigma). (5) U decay constants and composition as follows: ²³⁸U = 9.8485 × 10⁻¹⁰, ²³⁵U = 1.55125 × 10⁻¹⁰, ²³⁸U/²³⁵U = 137.88. (6) Analyses with >10% uncertainty (1-sigma) in ²⁰⁶Pb/²³⁸U age are not included. (7) Analyses with >10% uncertainty (1-sigma) in ²⁰⁶Pb/²⁰⁷Pb age are not included, unless ²⁰⁶Pb/²³⁸U age is <500 Ma. (8) Best age is determined from ²⁰⁶Pb/²³⁸U age for analyses with >10% uncertainty (1-sigma) in ²⁰⁶Pb/²³⁸U age <900 Ma and from ²⁰⁶Pb/²⁰⁷Pb age for analyses with >10% uncertainty (1-sigma) in ²⁰⁶Pb/²⁰⁷Pb age > 900 Ma. (9) Concordance is based on ²⁰⁶Pb/²³⁸U age/²⁰⁶Pb/²⁰⁷Pb age. Value is not reported for ²⁰⁶Pb/²³⁸U ages <500 Ma because of large uncertainty in ²⁰⁶Pb/²⁰⁷Pb age. (10) Analyses with ²⁰⁶Pb/²³⁸U age > 500 Ma and with >20% discordance (<80% concordance) are not included. (11) Analyses with ²⁰⁶Pb/²³⁸U age > 500 Ma and with >5% reverse discordance (<105% concordance) are not included. (12) Systematic errors are as follows (at 2-sigma level): [sample 1: 2.5% (²⁰⁶Pb/²³⁸U) & 1.4% (²⁰⁶Pb/²⁰⁷Pb)]. These values are reported on cells U1 and W1 of NUagecalc. (13) Analyses conducted by LA-MC-ICPMS, as described by *Gehrels et al.* [2008].

^bSample analyzed with Micromass Isoprobe multicollector inductively coupled plasma mass spectrometer (MC-ICPMS).

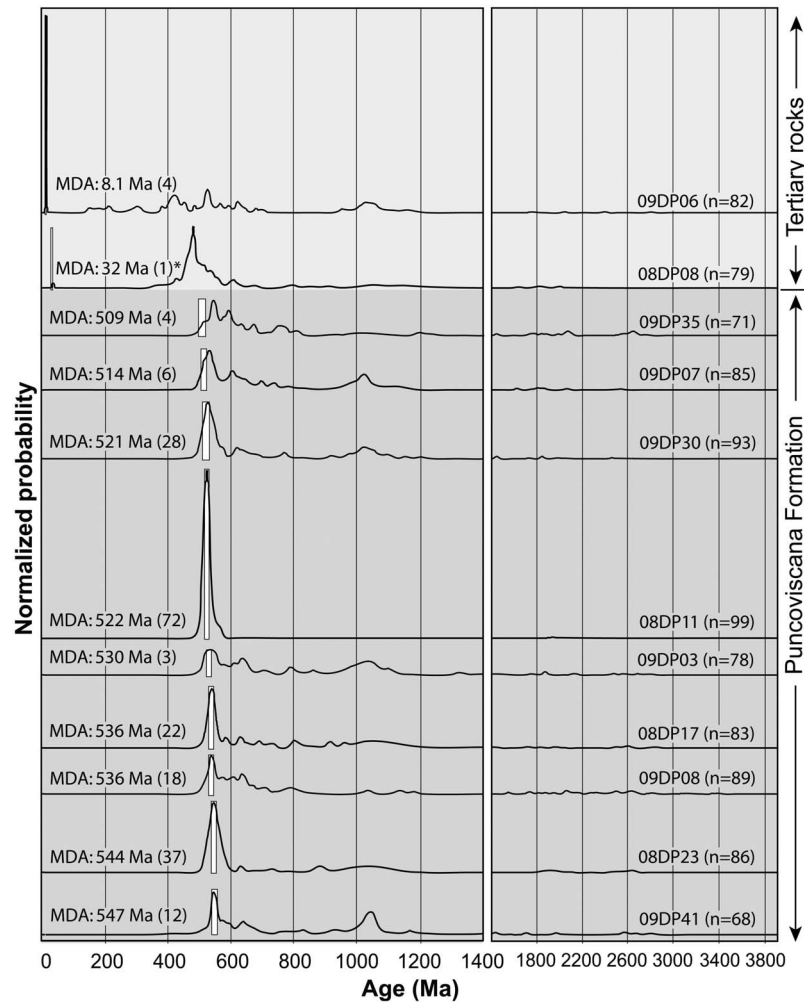


Figure 8. Normalized probability plots of detrital zircon samples from the Cachi Range. All samples except 08DP11 contain a Grenvillian age peak at ~ 1.05 Ga, with variable populations of younger, likely Brazilian/Pan-African ages. Most samples' zircon populations are dominated by Cambrian ages that are interpreted to indicate a more proximal source from coeval, Pampean arc magmatism. The age-probability diagrams show each age and its uncertainty (for measurement error only) as a normal distribution, and sum all ages from a sample into a single curve, using routines in Isoplot [Ludwig, 2001]. Composite age probability plots normalize each curve according to the number of constituent analyses such that each curve contains the same area, and then stacks the probability curves. MDA – Maximum depositional age. We assign MDAs to the youngest age cluster in a sample defined by three or more overlapping analyses [Dickinson and Gehrels, 2009]. For age probability peaks that comprise many grains, we use the age of the peak, unless a distinct younger population of grains is present. In parentheses next to the MDA is the number of overlapping and concordant analyses used to calculate the age. *Sample yielded only one Cenozoic age and therefore does not result in a statistically reliable MDA.

and deformation within the Cachi Range. Analytical details are available in Table 1.

5.2. U-Pb Detrital Zircon

5.2.1. Methods

[32] Detrital zircon (DZ) ages are shown on relative age-probability diagrams (Figure 8). For many samples from the Cachi Range, maximum depositional ages (MDAs) revealed by U-Pb DZ geochronology provide insight into the age and style of deformation events. A single zircon analysis may be

taken, in some cases, to constrain the maximum depositional age of a sedimentary rock. The more conservative approach taken here, however, allows for the interpretation that a single age may be compromised by Pb loss or inheritance. We therefore assign MDAs to the youngest age cluster in a sample defined by three or more overlapping analyses [Dickinson and Gehrels, 2009]. MDAs for rocks from the Puncoviscana Formation were projected onto structural cross sections of the Cachi Range to show spatial-temporal relationships among the DZ samples (Figure 9).

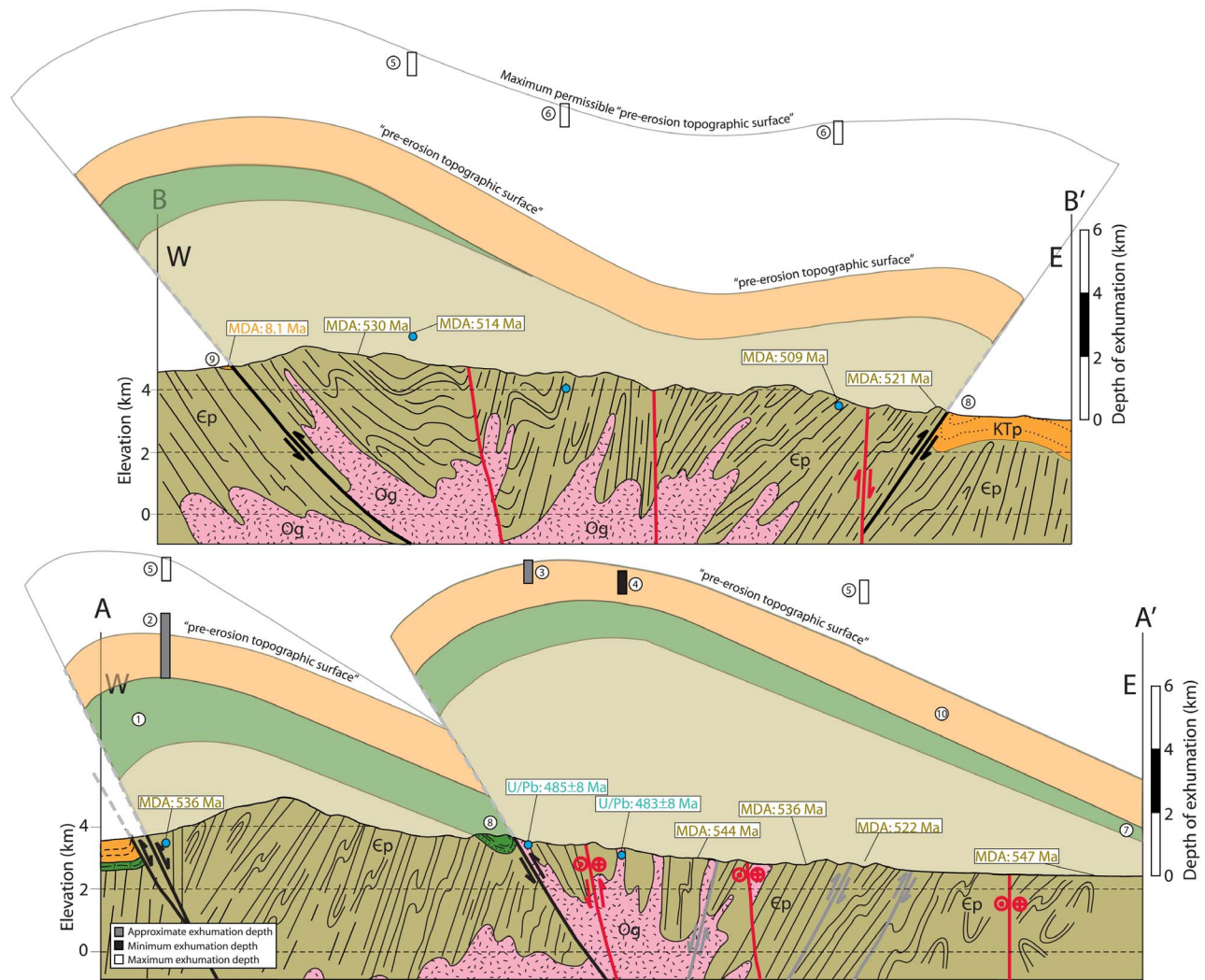


Figure 9. Schematic cross sections across the Cachi Range near the latitudes of (top) La Poma and (bottom) Cachi. Cross section locations and unit colors and symbols are shown in Figure 3. Gray subsurface faults are interpreted as Paleozoic structures, black are Cenozoic reverse faults, and red are more recent strike-slip faults. The pre-erosion topographic surface was constructed from geological constraints and estimates of depths of exhumation based upon the relative extent of resetting of (U-Th)/He zircon and apatite fission track (AFT) [Deeken *et al.*, 2006] samples, assuming a paleo-geothermal gradient of 20°C/km [cf. Deeken *et al.*, 2006]. Blue circles are sample locations. Circled numbers refer to specific constraints: 1) Maximum thickness of Pirgua near Brealito as constrained by Carrera *et al.* [2006]; 2) Approximate amount of exhumation constrained from thermal modeling of AFT data by Deeken *et al.* [2006]; 3) Approximate depth of exhumation; AFT is reset and (U-Th)/He in zircon is nearly reset; 4) Minimum depth of exhumation given reset (U-Th)/He in zircon; 5) Maximum depth of exhumation given unreset (U-Th)/He in zircon; moderate dispersion of individual grain ages indicates intermediate depth of exhumation; 6) Maximum depth of exhumation given unreset (U-Th)/He in zircon; major dispersion of individual grain ages indicates low magnitude of exhumation; 7) Approximate thickness and dip of Pirgua east of Cachi; 8) Overturned footwall syncline indicates fault propagation folding is important; 9) Off-set unit suggests thrust faulting occurred after ~8 Ma; and 10) Thickness is from preserved strata east of Cachi and exhumation depths where minimal Cenozoic erosion has occurred. Uniform thickness assumed for simplicity. Age-dating abbreviations – MDA: maximum depositional age from detrital zircon results; U/Pb: U-Pb zircon.

5.2.2. Results

[33] To discern relative ages of rocks juxtaposed across identified structures in the Cachi Range where Cenozoic rocks are absent, detrital zircon sampling was conducted along

transects across the range to yield MDAs of the Puncoviscana Formation. Given that the youngest zircon populations dominate nearly all DZ samples (Figure 8), we infer that there was a continuous supply of young zircons during deposition.

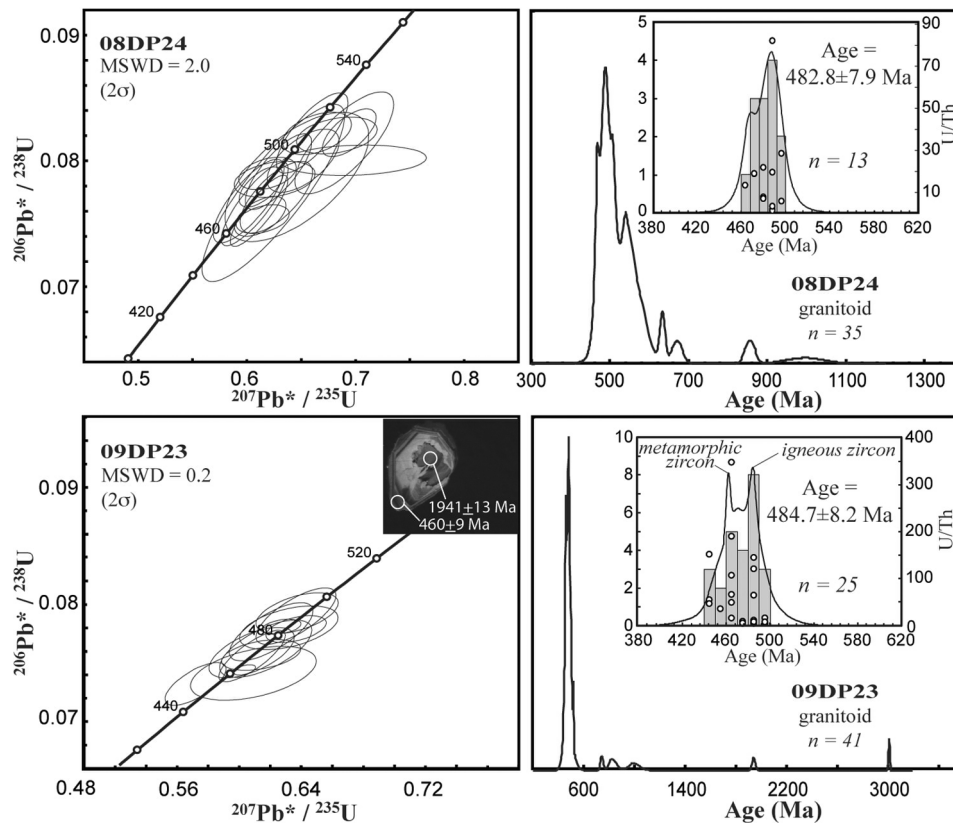


Figure 10. Concordia plots for rim zircon, with inset cathodoluminescence image showing different age domains in an individual zircon crystal. Also shown are probability plots for all zircon analyses demonstrating the presence of older, inherited components that are similar to detrital zircon populations observed in samples of the Cambrian Puncoviscana Formation, suggesting these rocks may have crystallized from melts derived from the Puncoviscana Formation. Concordia plots were constructed with Isoplot [Ludwig, 2001]. High U/Th in zircon rims of sample 09DP23 suggest that zircon grew in two stages: an original igneous crystallization event at ~ 485 Ma, followed by metamorphic zircon growth at ~ 462 Ma.

Because the youngest age peaks vary among samples, MDAs from most samples obtained from the Puncoviscana Formation are interpreted to approximate depositional ages, and represent deposition from 547 to 509 Ma. There is a general decrease in age from the core of the range to the east, consistent with structurally higher rocks being older than, and juxtaposed in thrust sense against structurally lower rocks by displacement within at least two W-dipping shear zones (gray structures in Figure 7). These rocks generally yielded younger MDAs than published DZ results, but are comparable to the youngest previously published age of ~ 520 Ma obtained from a sample of the Puncoviscana Formation collected from ~ 7 km south of Cachi by Adams *et al.* [2008].

[34] A Cenozoic sandstone sample (09DP06) offset by the Cachi fault at the northwestern range margin yielded a MDA of ~ 8 Ma, indicating that shortening on this fault persisted at least until late Miocene time. Another sample collected from the Quebrada de los Colorados Formation south of La Poma (Figure 5) yielded one zircon with an age of ~ 32 Ma, statistically insignificant, but consistent with continued deposition of this unit into Oligocene time, as Hongn *et al.* [2007] suggested.

5.3. U-Pb Igneous Zircon

5.3.1. Methods

[35] Two two-mica bearing granitoids from the Cachi Range were selected for U-Pb zircon analysis. Initial analyses from each igneous sample, aided by cathodoluminescence (CL) images, were conducted on cores and rims of zircons to assess intragrain age variability. One of these igneous samples (08DP24) was analyzed with a GVI *Isoprobe* with a laser spot size of $25 \mu\text{m}$. In contrast, analyses on igneous grains of sample 09DP23 were performed with a Nu HR ICP-MS, using a spot size of $30 \mu\text{m}$ for core analyses and $22 \mu\text{m}$ for rim analyses. CL images of these zircons show irregularly shaped zircon cores with dissolved margins, surrounded by euhedral, concentric-zoned rim overgrowths (Figure 10 inset). Zircon cores yielded highly variable, older ages relative to rims that are consistently Early to Middle Ordovician in age (timescale used throughout this paper is of Ogg *et al.* [2008]) and likely represent the age of pluton crystallization. Further analyses were therefore conducted on zircon rims to obtain representative ages.

[36] In addition to analytical uncertainties (see Table 1), age uncertainties of magmatic and metamorphic zircon also

arise from data sets complicated by older inherited zircon, lead loss, or new zircon growth. To minimize errors resulting from inclusion of inappropriate analytical data in age calculations, we report weighted means [Ludwig, 2001] of concordant and overlapping $^{206}\text{Pb}/^{238}\text{U}$ ages for igneous samples, with final uncertainties that include all random and systematic errors. Interpreted crystallization ages are reported with 2σ uncertainties on concordia diagrams (Figure 10 and Table 1).

5.3.2. Results

[37] Concordia plots, weighted mean ages, and U/Th versus age for rim analyses of igneous samples are shown on Figure 10 (see also Table 1). Zircon cores with a high degree of inheritance have implications for the geological history of these rocks. Based on field observations in the area that indicate high-grade metamorphism and anatexis of metasedimentary rocks, we suggest that plutons dated here were derived from partial melting of a Puncoviscana-like source, with additional input from more mafic and/or underplated lower crustal rocks [Méndez et al., 2006]. The presence of inherited zircons that are similar in age to those obtained from Puncoviscana samples elsewhere in the Cachi Range support this assertion (Figures 8 and 10). Rim analyses, on the other hand, yielded reproducible ages between 485 and 462 Ma. Younger rim ages for sample 09DP23 generally correspond to higher U/Th ratios; although there is some overlap, this hints at an earlier, ~ 485 Ma crystallization age and a younger, ~ 462 Ma metamorphic overgrowth. These Ordovician ages overlap with previous U-Pb zircon crystallization ages for Famatinian rocks to the south [e.g., Dahlquist et al., 2008; Ducea et al., 2010], and reflect short-lived Ordovician magmatism. Our ~ 462 Ma zircon rims interpreted to be a result of additional, later metamorphic overgrowth are consistent with ~ 470 – 455 Ma U-Pb monazite and titanite ages interpreted to record high-grade metamorphism ~ 100 km to the south [Büttner et al., 2005].

6. (U-Th)/He Zircon Thermochronology

6.1. (U-Th)/He Zircon

6.1.1. Methods

[38] Sorting out different ages of deformation within pre-Mesozoic rocks to estimate the magnitude of Cenozoic shortening is a challenge in northwestern Argentina where older Paleozoic shortening is prevalent. To circumvent this problem, we used (U-Th)/He zircon thermochronology to obtain constraints on the timing and magnitude of rock exhumation. (U-Th)/He thermochronometry of zircon generally reflects the time since cooling of the zircon below $\sim 180^\circ\text{C}$ (assuming an effective grain radius of $60\ \mu\text{m}$ and a cooling rate of $10^\circ\text{C}/\text{Ma}$ [Reiners, 2005]).

[39] Deeken et al. [2006] used AFT ages from vertical transects in the Cumbres de Luracatao (Figure 1) to obtain a Miocene geothermal gradient of $\sim 18^\circ\text{C}/\text{km}$. While we recognize that foreland basins typically have low geothermal gradients ($\sim 22^\circ\text{C}/\text{km}$ [Allen and Allen, 1990]), we believe that $18^\circ\text{C}/\text{km}$ may underestimate the true paleo-geothermal gradient and have instead elected to use a slightly higher geothermal gradient of $20^\circ\text{C}/\text{km}$. Given a mean annual surface temperature of $10 \pm 5^\circ\text{C}$, the $\sim 180^\circ\text{C}$ blocking

temperature of the (U-Th)/He zircon system yields closure depths of 8–9 km. For previously published apatite fission track (AFT) results [Deeken et al., 2006], the corresponding closure depths are ~ 3.5 – 7 km [Reiners and Brandon, 2006]. A higher geothermal gradient would decrease exhumation depths and interpreted fault offsets.

[40] Regionally contiguous marine-influenced strata of the Cretaceous Salta Group provide an “undeformed” datum near sea level that existed in the region prior to formation of the Andes, when regional isotherms were probably flat. Therefore, Cenozoic thermochronological ages provide minimum estimates of the amount of structural relief (exhumation magnitude + relief above regional elevation of Cretaceous limestones) generated since the Cretaceous. We assume that exhumation indicated by thermochronological results reflects erosional unroofing during fault displacement. We supplement earlier work in the region [e.g., Coutand et al., 2001; Deeken et al., 2006] by focusing on systematic relationships among faults and ages of low temperature thermochronometers in the Cachi Range.

[41] We performed (U-Th)/He zircon thermochronometry on seven samples (five meta-sedimentary and two igneous); five of these samples utilized half-grains previously dated by the LA-ICP-MS U-Pb technique described above (see Reiners et al. [2007] for alpha-ejection corrections on half grains). To assess the degree of equilibration with respect to (U-Th)/He in zircon within samples, four grains were dated for four of the samples, while three grains were dated from the other three samples (Table 2).

6.1.2. Results

[42] One (U-Th)/He zircon sample from the Cachi Range (09DP37; northwestern sample in Figure 5) yielded a strong inverse age-U concentration correlation (Table 2), likely a result of radiation damage effects on He diffusivity in zircon [Reiners, 2005]. Radiation damage effects in zircons often require old ages, relatively high U-Th concentrations, and imply long-term residence of zircons at temperatures insufficient to anneal alpha recoil damage zones [Reiners, 2005].

[43] In the southern transect, one sample yielded a consistent population of mid-Miocene ages (~ 15 Ma; Figure 7). An additional sample ~ 3 km west of this yielded mid-Miocene ages that are not statistically overlapping, but were nearly completely reset during mid-Miocene exhumation. These two samples were collected from the hanging wall of the Las Cuevas fault in the core of the Cachi Range (Figure 7), and are consistent with ~ 8 – 10 km of exhumation here, at or since 15 Ma. The two existing AFT ages from the Cachi Range also yielded mid-Miocene ages (~ 15 Ma [Deeken et al., 2006]); identical (U-Th)/He zircon ages imply rapid exhumation associated with shortening during mid-Miocene time.

[44] The lack of complete resetting in the (U-Th)/He zircon system in five additional samples collected from the margins of the mountain range demonstrates that at these localities, the range did not undergo the 8–9 km of exhumation at or since 15 Ma (Figures 5–7 and 9) required to bring to the surface the $\sim 180^\circ\text{C}$ isotherm that represents the temperature below which He is diffusionally retained in zircon. Although our current understanding of He diffusion in zircon is insufficient to extract high quality quantitative

Table 2. (U-Th)/He Ages for Individual Zircons From the Cachi Range^a

Sample	U (ppm)	Th (ppm)	Th/U (atomic)	⁴ He (nmol/g)	Mass (μ g)	Half-Width (μ m)	HAC (Ft)	Corrected Age (Ma)	$\pm 2\sigma$ Analyt. Error
08DP11 (25.10293°S, 66.245050°W)									
Grain									
08DP11-10-zr	412	220	0.63	96.2	1.87	32.8	0.752	57.3	2.5
08DP11-35-zr	326	182	0.66	186	14.1	61.8	0.871	120	5.3
08DP11-80-zr	505	312	0.74	104	5.76	44.0	0.819	46.5	2.0
08DP24 (25.09127°S, 66.298067°W)									
Grain									
08DP24-10-zr	417	83.4	0.22	24.5	1.25	27.0	0.734	14.9	0.71
08DP24-13-zr	278	103	0.42	18.2	1.51	26.3	0.729	16.6	0.78
08DP24-15-zr	340	105	0.34	21.6	1.40	30.0	0.747	15.8	0.78
09DP07 (24.714453°S, 66.418003°W)									
Grain									
09DP07-54-zr	445	170	0.43	69.8	1.30	27.0	0.638	40.2	2.5
09DP07-87-zr	575	214	0.42	93.5	1.92	28.8	0.637	40.9	2.5
09DP07-91-zr	215	103	0.55	58.6	0.78	23.3	0.568	75.0	4.2
09DP07-100-zr	193	79.2	0.47	40.5	5.18	48.0	0.766	46.9	3.1
09DP08 (25.137981°S, 66.433907°W)									
Grain									
09DP08-48-zr	456	178	0.44	96.3	2.75	33.0	0.711	50.6	3.4
09DP08-69-zr	407	289	0.87	116	1.86	31.8	0.683	70.1	4.6
09DP08-78-zr	166	103	0.75	31.0	1.17	27.0	0.627	48.1	3.2
09DP08-92-zr	275	98.6	0.40	75.6	5.01	47.3	0.771	61.7	4.1
09DP35 (24.657707°S, 66.256599°W)									
Grain									
09DP35-71-zr	114	44.9	0.44	191	3.28	37.5	0.706	384	26
09DP35-82-zr	220	69.9	0.35	69.9	2.26	32.0	0.694	77.1	5.3
09DP35-84-zr	171	56.3	0.37	101	3.76	34.0	0.710	139	9.0
09DP35-85-zr	491	133	0.30	149	4.04	38.8	0.745	70.4	4.1
09DP23 (25.088527°S, 66.328176°W)									
Grain									
09DP23-zr-1	242	137	0.67	15.8	2.95	32.0	0.705	17.2	1.0
09DP23-zr-2	295	99.2	0.37	25.4	4.17	34.3	0.729	21.9	0.73
09DP23-zr-3	289	66.6	0.25	38.8	6.00	48.5	0.785	31.7	2.0
09DP37 (24.644486°S, 66.29634°W)									
Grain									
09DP37-zr-1	3650	467	0.14	54.9	0.48	17.8	0.500	5.58	0.29
09DP37-zr-2	1140	132	0.12	162	3.13	38.5	0.736	35.7	2.0
09DP37-zr-3	536	141	0.29	181	2.06	31.8	0.692	90.3	5.3
09DP37-zr-4	44.2	18.0	0.46	157	1.64	30.0	0.669	931	56

^a2 σ represents formal analytical error of individual runs.

thermal histories from grains that are incompletely reset, this lack of complete resetting places a maximum constraint upon the depth of exhumation of these partially reset samples. Samples with old, highly variable individual grain ages were not subjected to very high temperatures during Neogene time and likely represent shallower depths of erosion, whereas samples that yield consistently young individual grain ages with less dispersion were more completely reset and underwent greater Neogene exhumation. Along with geological constraints, these estimates are incorporated into our schematic cross sections that help constrain the geometry of fault hanging walls where Cretaceous and Cenozoic strata were eroded (Figure 9). In general, older (U-Th)/He zircon and AFT ages obtained from samples collected farther from reverse faults demonstrate that significant exhumation was localized to the

proximal hanging walls of E-dipping Cenozoic reverse faults (Figure 9).

7. Discussion

7.1. Puncoviscana and Early Paleozoic Tectonics

[45] The abundance of Cambrian zircons in our samples of the Puncoviscana Formation supports *Adams et al.*'s [2011] assertion that a magmatic arc became active in the region during Cambrian time. This implies that the initial passive margin depositional setting of the Puncoviscana Formation evolved during Cambrian time to an active subduction margin. Major shortening by syndepositional folding of this age in the Puncoviscana Formation ($\geq 50\%$ [*Piñán-Llamas and Simpson, 2006*]) is likely related to convergence above this incipient subduction zone.

[46] Our youngest MDA from Puncoviscana rocks (Figure 8) was obtained from the northern Cachi Range and constrains the end of major Cambrian shortening to after ~509 Ma, significantly younger than previously published DZ results. Deposition of the Puncoviscana until ≤ 509 Ma requires that the intrusion of Pampean granitoids from 526 to 517 Ma [Hongn *et al.*, 2010] was syndepositional. An observed lack of deformation in Cambrian granitoids may reflect episodic shortening events in the Puncoviscana Formation and/or a weaker rheology of the Puncoviscana Formation relative to stronger granitoids.

[47] U-Pb igneous zircon results establish magmatism in the core of the Cachi Range at ~485 Ma. We infer a metamorphic event at ~462 Ma, based on U-Pb ages of thin metamorphic rims around inherited zircon cores, which may reflect the culmination of Ordovician metamorphism/orogenesis. Field observations and MDA U-Pb zircon results of samples collected from the Puncoviscana Formation also imply significant crustal shortening accommodated by N-S striking, W-dipping ductile shear zones. Brittle faulting has only locally modified this dominant, commonly ductile fabric, and there is a distinct difference among foliation attitudes measured near and within Ordovician granitoids (W-dipping) and bedding, bedding parallel cleavages, and primary cleavages obtained from the Cambrian Puncoviscana Formation (generally NW- to SE-dipping; Figure 3). These observations suggest that N-S striking, penetrative fabrics in the core of the range reflect Ordovician shortening. We are unable to constrain whether this shortening occurred before, during, or after high-grade metamorphism that accompanied arc magmatism. However, a normal-sense, ultramylonitic shear zone postdates the granitoid in which it formed; we speculate that the structure accommodated post-orogenic collapse of an Ordovician mountain belt. Ordovician deformation and metamorphism have been recognized across much of Argentina and have been attributed to the cessation of Famatinian magmatism caused by the accretion of the Precordillera terrane [Rapela *et al.*, 1998; Astini and Dávila, 2004; Ducea *et al.*, 2010].

[48] In summary, the Puncoviscana Formation is locally of demonstrable Middle Cambrian age and was intruded by mainly Early Cambrian plutons. Subsequently, it was overlain by the Late Cambrian Mesón Group [Adams *et al.*, 2011] and intruded by Early Ordovician plutons (Figure 2). These temporal relationships are consistent with a tectonically active plate margin in the early Paleozoic. Coupled with previously published results, data from this study suggest that “Pampean” and “Famatinian” orogenesis are not temporally distinct orogenic events, but rather represent continuous orogenesis at the plate margin (≥ 550 to ~465 Ma [Lucassen *et al.*, 2000; Ducea *et al.*, 2010; Adams *et al.*, 2011, and references therein; this study]) punctuated by a rather brief period from ~509 to ≥ 492 Ma [Adams *et al.*, 2011; this study] during which there was significant post-depositional shortening, uplift, and erosion of the Puncoviscana Formation and regional deposition of the Mesón Group.

7.2. Influence of Salta Rift Structures on Cenozoic Shortening

[49] The Cachi fault (Figure 3) is interpreted to be a reactivated normal fault that accommodated crustal

thickening related to uplift of the Cachi Range. We infer that the overall geometry of Cenozoic reverse structures within the range was controlled by preexisting extensional heterogeneities. In particular, in the north of the Cachi Range where there is no evidence of Cretaceous extension, range-bounding shortening structures are bi-vergent. To the south, however, these bi-vergent structures transition to dominantly W-vergent structures where the E-dipping Cachi fault is demonstrably an inverted normal fault. The overall geometry of this southward transition may reflect a pre-existing extensional fault step-over or may reflect the increased importance of pre-Cenozoic weaknesses in controlling the locations of Cenozoic shortening structures. The small magnitude of Cretaceous extension in the region [e.g., Grier *et al.*, 1991] probably also predisposed a much more heterogeneous pattern of Cenozoic shortening relative to thin-skinned thrusting in Bolivia, as reactivation of discontinuous structures resulted in strong along-strike gradients in structural relief along individual structures.

7.3. Magnitude and Style of Cenozoic Shortening

[50] Our results show that Miocene exhumation in the Cachi Range was significant (up to 10 km) and spatially controlled by deformation related to mainly E-dipping reverse faults. Although the greatest magnitude of exhumation occurred in the hanging wall of the Las Cuevas fault, the sample closest to the fault is less deeply exhumed than a sample collected ~3 km farther east of the fault (Figures 7 and 9). This is consistent with field observations in the region of steep to overturned footwall synclines subjacent to wide zones (≤ 200 m) of distributed fracturing of hanging wall Puncoviscana Formation, suggesting a fault-propagation style of folding (Figures 4, 9, and 11). A general decrease in magnitude of exhumation away from fault traces also implies fault-bend folding resulting from faults that shallow with depth.

[51] A fold above the propagating tip of a reverse fault forms because slip along the discrete fault at depth does not instantaneously propagate to the surface; instead, displacement accommodated by faulting at depth occurs by folding above the fault tip [Williams and Chapman, 1983; Erslev, 1991]. The resultant slip gradient along the fault is such that displacement across the fault increases with depth, while significant structural relief at the surface is accomplished by folding, with little or no fault offset at shallow crustal levels [e.g., Erslev, 1991; Allmendinger, 1998]. Recognition of this style of deformation is important in attempts to quantify regional shortening magnitudes; consideration of only fault slip at the surface to constrain shortening will significantly underestimate the true magnitude of shortening.

[52] Major Neogene exhumation in the Cachi Range is in contrast to a lack of major Neogene exhumation within the rest of the thrust belt at this latitude (22–26°S), which is demonstrated by a suite of (U-Th)/He zircon samples collected across the orogen that yield ages >100 Ma [Reiners *et al.*, 2010]. Given the likelihood that major exhumation reflects erosional unroofing during fault displacement, this suggests that faults within the Cachi Range accommodated the growth of relatively more structural relief than other faults at this latitude. One argument for the observed “deficit” in shortening in northwestern Argentina [e.g., Kley and Monaldi, 1998] contends that significant faulting at deeper

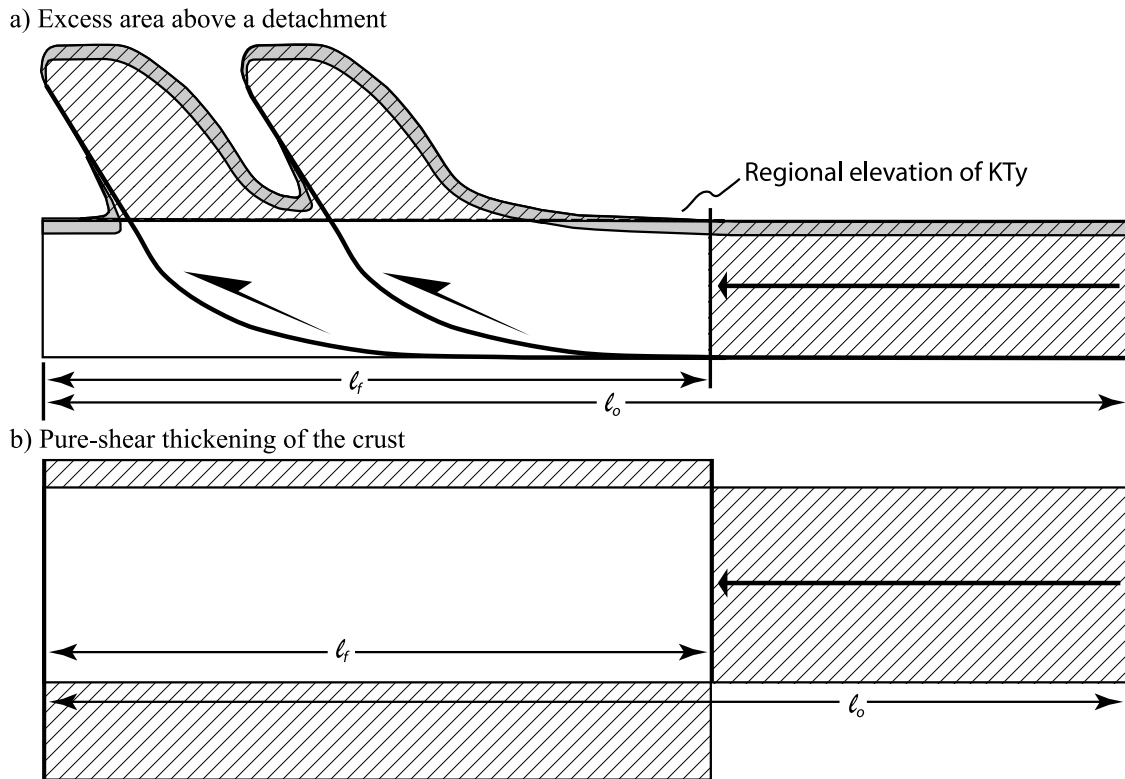


Figure 11. Schematic cartoons of methods used for calculating the magnitude of shortening in the Cachi Range. Line fill indicates that shortened area is equal to area of deformed section. (a) Excess area above an upper crustal décollement. (b) “Pure-shear” thickening of the entire crust.

structural levels that is necessarily accommodated at shallower levels may be localized across narrow zones rather than distributed across many structures in the thrust belt (e.g., passive roof duplexing). Evaluation of the magnitude of shortening accommodated by the most deeply exhumed portion of the thrust belt therefore provides a unique scenario in which to test whether such a model is applicable to the thrust belt at this latitude. In other words, can shortening within the most deeply exhumed portion of the thrust belt where the greatest magnitude of Neogene shortening was accommodated account for the discrepancy in the predicted versus observed magnitude of shortening?

[53] Provided that up to 10 km of rapid exhumation occurred in the Cachi Range at or since ~ 15 Ma, we assume that partially reset (U-Th)/He zircon samples with variable individual grain ages older than ~ 15 Ma are less deeply exhumed than fully reset samples. This provides a minimum and maximum depth of exhumation for reset and partially reset samples, respectively (8–9 km). The same reasoning applies to published AFT ages [Deeken *et al.*, 2006] that record shallower depths of erosion. In this way, we approximated the magnitude of exhumation above reverse faults in the Cachi Range; coupled with field observations of the style of deformation near reverse faults and hanging wall geometries of deformed Cenozoic rocks southeast of Cachi, we estimated the first order deformed geometry of the “pre-erosion” surface above the Cachi Range (Figure 9). This allows us to evaluate the amount of structural relief and magnitude of shortening that was accommodated by these faults. To this end, we assumed that the excess cross-

sectional area of rock displaced above a regional reference horizon (in our case, the regional-scale, marine-influenced Yacoraite Formation) is equal to the area of rock translated during fault displacement (Figure 11a). By assuming a reasonable décollement depth, which can be estimated by the wavelengths of fault-bend folds in deformed thrust sheets, it is possible to calculate the magnitude of shortening accommodated by Cenozoic reverse faults in the Cachi Range.

[54] In our southern transect (Figure 7), eastward-decreasing depths of exhumation in fault hanging walls are inferred to represent fault-bend folding (Figure 9) and constrain the décollement depth. Using the cross section balancing software 2DMove, we forward modeled fault geometries that satisfy the back-limb dips constrained from Cretaceous and Cenozoic rocks southeast of Cachi and “pre-erosion” surfaces estimated from decreasing depths of exhumation from our thermochronological results (Figure 9). Fault-bend folds produced from these forward models suggest that the original décollement depth beneath the Yacoraite Formation was between 10 and 15 km. This is in agreement with a regional excess area calculation across the Eastern Cordillera and Santa Bárbara Ranges at this latitude using the line-length method of *Dahlstrom* [1969] that yields an original décollement depth of ~ 14 km, as well as *Grier et al.*'s [1991] balanced section to the southeast that used a décollement depth of 10–12 km. We note that a deeper décollement would result in a decreased magnitude of shortening for a given excess area. We measured the excess areas beneath our best estimate of the “pre-erosion” surface (Figure 9) relative to 2500 and 2900 m (southern and

northern transects, respectively), which are the modern elevations of Balbuena limestones exposed in the Valle de Calchaquí to the east. To encompass a reasonable range of uncertainty, we also measured the excess area defined by a maximum “pre-erosion” surface that represents that absolute maximum magnitude of Neogene exhumation that could have occurred above (U-Th)/He zircon samples that are incompletely reset (Figure 9). To allow for the possibility that the Yacoraite Formation preserved subjacent to the Cachi Range has been deformed above its “undeformed” reference horizon, we used a regional elevation of -2000 m above which to measure the excess areas, which is the deepest elevation of the undeformed Yacoraite Formation in minimally deformed synclines in the Santa Bárbara Ranges [Kley and Monaldi, 2002].

[55] Using our estimate of the original décollement depth of 10–15 km, the Cenozoic structural relief from our best estimate of the “pre-erosion” surface in the Cachi Range (Figures 9 and 11) yields 20–8 km of shortening, whereas our maximum estimate of the excess area yields 44–25 km of shortening across the width of the Cachi Range. The maximum possible magnitude of shortening accommodated by what is likely the most deeply exhumed portion of the thrust belt in this region is therefore $\sim 28\%$ of the ~ 160 km shortening magnitude “discrepancy” that has been suggested for this latitude [e.g., Kley and Monaldi, 2002]. Although an updated balanced cross section across the thrust belt at this latitude is required to more rigorously evaluate the likelihood of additional shortening, the moderate magnitude of shortening implied by our results in the Cachi Range suggests that existing assessments of the shortening magnitude in northwestern Argentina are not grossly underestimated. Therefore, we conclude that the observed along-strike change in shortening magnitude [e.g., Isacks, 1988; Kley and Monaldi, 1998] is real.

[56] Despite the moderate magnitude of Cenozoic shortening, the Cachi Range stands at high elevation (up to 6380 m) and is underlain by a thick crust (~ 58 km [Yuan et al., 2002; Wölbern et al., 2009]). The crustal thickness of the Cachi Range prior to Cenozoic shortening was likely similar to that in the modern foreland east of the Andes, which is ~ 35 km [Beck and Zandt, 2002; Yuan et al., 2002]. On average, ~ 5 km of material was eroded from above the Cachi Range since the Miocene based on our thermochronological results, suggesting that a ~ 63 -km-thick column of crust must be accounted for. Our work suggests that folding and faulting above an originally 10–15 km deep décollement resulted in uplift of rocks above their regional, undeformed level. If we consider this regional reference to be at an elevation of -2000 m, then the maximum height of our “pre-erosion” topographic surface above this reference elevation is ~ 15 km, which is the maximum amount that the crust was thickened. This is $\sim 60\%$ of the 25 km of thickening required for the crust to attain its observed thickness. Previous authors have suggested that deeply rooted faults could account for this discrepancy in crustal thickness and shortening [e.g., Allmendinger and Gubbels, 1996], but our results suggest that deformation in the Cachi Range was mainly accommodated by a detachment at a moderate depth. Under the assumption of pure-shear crustal thickening, the amount of shortening across the width of the Cachi Range (35–42 km) required to thicken the entire crust from an

original thickness of 35 km to ~ 63 km is 28–34 km (Figures 9 and 11b). This is within the upper range calculated with our excess area method above for the upper crust. Assuming that the estimation of the Moho depth in the region is accurate, this suggests that the observed “excess” in crustal thickness beneath the Cachi Range could be explained by sub-décollement pure-shear thickening of the crust concurrent with upper crustal folding and faulting. Although crustal addition by other mechanisms (e.g., crustal flow, magmatic underplating) could account for the “excess” crust beneath the Cachi Range, our field observations suggest that the fine-grained Puncoviscana Formation is highly susceptible to penetrative strain by formation of pressure solution cleavage. We also acknowledge the possibility that the redistribution of tectonically underthrust crust at the eastward-migrating subduction margin may have resulted in underplating beneath the hinterland, particularly during periods of shallow subduction [e.g., Ramos, 2009].

[57] Recent analysis of internal strain in rocks from the Wyoming salient of the western North American thrust belt demonstrates that regions with thinner initial basin strata at salient margins correspond to relatively less fault slip and overall shortening but greater internal strain accommodation; this is likely due to decreased fault slip near basin margins that led to increased local stress [Weil et al., 2010; Yonkee and Weil, 2010]. We propose that a similar scenario on a more regional scale is encountered in the southern central Andes, where the presence of a thick Paleozoic basin permitted major thin-skinned shortening in Bolivia, flanked in northern Argentina by a significantly thinner pre-Cenozoic framework [Allmendinger and Gubbels, 1996]. Relative to southern Bolivia, rocks in northwestern Argentina were less susceptible to major shortening by faulting due to the strain-hardened nature of the low-grade metamorphic basement. Instead, existing steeply dipping heterogeneities were reactivated, and the fine-grained nature of the rocks and higher stress in the thrust belt may have resulted in a greater role for penetrative strain in accommodating sub-décollement thickening of the crust. Previous researchers have demonstrated that significant shortening was accommodated by penetrative strain in other orogens worldwide, including western North America [e.g., Mitra, 1994; Duebendorfer and Meyer, 2002; Yonkee and Weil, 2010], and southwestern China [e.g., Burchfiel et al., 2007].

7.4. Transition to Strike-Slip Faulting

[58] East of the Puna Plateau in northwestern Argentina, major shortening occurred at ~ 20 Ma in the Cumbres de Luracatao [Deeken et al., 2006] and then stepped eastward into the Cachi Range at ~ 15 Ma, where shortening continued until ≤ 8 Ma (this study). This was then followed by foreland-ward propagation of deformation to the Santa Bárbara Ranges (< 10 Ma to Present [Reynolds et al., 2000]). This late Miocene eastward propagation of deformation was followed by a change in stress state. Quaternary deformation in the Cachi Range is characterized by sinistral strike-slip faulting that has reactivated and locally offset older, shortening-related faults and folds. This change in stress state occurred after ~ 8 Ma because reverse faulting was active at this time at the northwestern margin of the Cachi Range. This was also a regional-scale event, given that Quaternary strike-slip faults have also been identified ~ 125 km east of the

Cachi Range in the Quebrada del Toro [e.g., Marrett *et al.*, 1994], and normal faults have initiated since 3.5 to 7 Ma in the southern Puna Plateau [Schoenbohm and Strecker, 2009]. The change in stress state is consistent with an increase in gravitational potential energy; the spatial association of late Cenozoic mafic magmatism demonstrates local melting of mantle material. Both may be explained by removal of mantle lithosphere from beneath the orogen [Kay *et al.*, 1994; Schoenbohm and Strecker, 2009]. Lithospheric removal may also have placed the retroarc thrust belt into a supercritical state of taper [DeCelles *et al.*, 2009] and thereby explain the rapid >150 km eastward propagation in thrusting from the Cachi Range to the Santa Bárbara Ranges since 8 Ma.

8. Conclusions

[59] Cambrian zircons dominate U-Pb detrital zircon age populations in the Puncoviscana Formation within the Cachi Range. This implies that, following deposition in an originally passive margin setting, a magmatic arc became active in the region during Early to Middle Cambrian time. Subsequently, the Cachi Range underwent major, E-verging, Cambro-Ordovician shortening, ~485–483 Ma magmatism, ~462 Ma high-grade metamorphism, and possible orogenic collapse accommodated on extensional ductile shear zones.

[60] The style and magnitude of Cenozoic retroarc shortening in northwestern Argentina differs markedly from deformation within the thrust belt of Bolivia. Deformation in this part of Argentina was accommodated on moderately to steeply dipping reverse faults, involves reactivation of Cretaceous rift faults, and accommodated a lower magnitude of shortening than the thin-skinned thrust belt to the north. Rapid exhumation along two regional scale, W-verging reverse faults (likely reactivated Cretaceous normal faults) occurred in mid to late Miocene time (~15 to <8 Ma).

[61] (U-Th)/He zircon results demonstrate that up to 10 km of exhumation occurred in the Cachi Range, associated with mainly W-vergent fault-propagation folding. Using geological and thermochronological constraints in the Cachi Range, we reconstructed a “pre-erosion” topographic surface to evaluate the magnitude of shortening accommodated in one of the most deeply exhumed portions of the retroarc thrust belt at this latitude. The moderate magnitude of shortening that we extract from this work challenges the possibility of major crustal thickening by buried passive roof duplexing and suggests that while there is probably more shortening in this region than has been previously documented [e.g., Grier *et al.*, 1991], the major along-strike gradient in shortening in the central Andes is real. Coupled with previous results, our work also suggests that the moderate magnitude of shortening in the Eastern Cordillera at this latitude cannot produce the observed thick crust by upper-crustal shortening alone. Instead, penetrative strain and tectonic underplating of forearc rocks may help reconcile the thick crust beneath the Eastern Cordillera. Together with heterogeneities produced by rift structures during the Cretaceous, the style of shortening and crustal thickening in northwestern Argentina was likely controlled by the lack of a thick layer-cake stratigraphy and the predominance of previously deformed Puncoviscana metaturbidites, susceptible to a basement-involved style of deformation. After Miocene shortening in the Cachi Range, the stress state changed from one suitable for thrusting to

strike-slip faulting, possibly in response to lithosphere removal and an associated increase in gravitational potential energy. Our results have broad implications for contractional mountain belts, demonstrating that the pre-existing stratigraphic and structural architecture strongly influences the style and magnitude of shortening during later deformation and stress state changes may be common in regions of highly thickened and/or uplifted continental crust.

[62] **Acknowledgments.** This research was conducted as part of the Convergent Orogenic Systems Analysis (COSA) project, in collaboration with and funded by ExxonMobil. NSF grant EAR-0732436 is acknowledged for support of the Arizona LaserChron Center. D.P. acknowledges additional small grants and scholarships that helped fund this research from the Geological Society of America, ChevronTexaco, and ExxonMobil. Midland Valley generously provided 2DMove software to the University of Arizona. This work benefited from discussions with many people, including Facundo Fuentes, Ross Waldrip, Mike McGroder, Peter DeCelles, Gary Gray, Tom Becker, and Jerry Kendall. Detailed reviews by Jonas Kley and Nadine McQuarrie and anonymous comments on an earlier version significantly improved the manuscript.

References

- Aceñolaza, F. G., H. Miller, and A. Toselli (1988), The Puncoviscana formation (Late Precambrian - Early Cambrian) - Sedimentology, tectonometamorphic history and age of the oldest rocks of NW Argentina, *Lect. Notes Earth Sci.*, 17, 25–37.
- Adams, C. J., H. Miller, A. J. Toselli, and W. L. Griffin (2008), The Puncoviscana Formation of northwest Argentina: U-Pb geochronology of detrital zircons and Rb-Sr metamorphic ages and their bearing on its stratigraphic age, sediment provenance and tectonic setting, *Neues Jahrb. Geol. Palaeontol. Abh.*, 247(3), 341–352.
- Adams, C. J., H. Miller, F. G. Aceñolaza, A. Toselli, and W. L. Griffin (2011), The Pacific Gondwana margin in the late Neoproterozoic-early Paleozoic: Detrital zircon U-Pb ages from metasediments in northwest Argentina reveal their maximum age, provenance and tectonic setting, *Gondwana Res.*, 19(1), 71–83, doi:10.1016/j.gr.2010.05.002.
- Allen, P. A., and J. R. Allen (1990), *Basin Analysis, Principles and Applications*, Blackwell, Oxford, U. K.
- Allmendinger, R. W. (1998), Inverse and forward numerical modeling of trishear fault-propagation folds, *Tectonics*, 17(4), 640–656.
- Allmendinger, R. W., and T. Gubbels (1996), Pure and simple shear plateau uplift, Altiplano-Puna, Argentina and Bolivia, *Tectonophysics*, 259(1–3), 1–13.
- Allmendinger, R. W., V. A. Ramos, T. E. Jordan, M. Palma, and B. L. Isacks (1983), Paleogeography and Andean structural geometry, north-west-Argentina, *Tectonics*, 2(1), 1–16.
- Allmendinger, R. W., M. Strecker, J. E. Eremchuk, and P. Francis (1989), Neotectonic deformation of the southern Puna Plateau, northwestern Argentina, *J. South Am. Earth Sci.*, 2(2), 111–130.
- Astini, R. A., and F. M. Dávila (2004), Ordovician back arc foreland and Ocolytic thrust belt development on the western Gondwana margin as a response to Precordillera terrane accretion, *Tectonics*, 23, TC4008, doi:10.1029/2003TC001620.
- Baby, P., P. Rochat, G. Mascle, and G. Herail (1997), Neogene shortening contribution to crustal thickening in the back arc of the Central Andes, *Geology*, 25(10), 883–886.
- Barnes, J. B., T. A. Ehlers, N. McQuarrie, P. B. O’Sullivan, and S. Tawackoli (2008), Thermochronometer record of central Andean plateau growth, Bolivia (19.5°S), *Tectonics*, 27, TC3003, doi:10.1029/2007TC002174.
- Beck, S. L., and G. Zandt (2002), The nature of orogenic crust in the central Andes, *J. Geophys. Res.*, 107(B10), 2230, doi:10.1029/2000JB000124.
- Bosio, P. P., J. Powell, C. del Papa, and F. Hongn (2009), Middle Eocene deformation-sedimentation in the Luracatao Valley: Tracking the beginning of the foreland basin of northwestern Argentina, *J. South Am. Earth Sci.*, 28(2), 142–154.
- Burchfiel, B. C., C. Studnicki-Gizbert, J. W. Geissman, R. W. King, Z. Chen, L. Chen, and E. Wang (2007), How much strain can continental crust accommodate without developing obvious through-going faults?, in *Whence the Mountains? Inquiries Into the Evolution of Orogenic Systems: A Volume in Honor of Raymond A. Price*, edited by J. W. Sears, T. A. Harms, and C. A. Evenchick, *Spec. Geol. Soc. Am.*, 433, 51–61.
- Büttner, S. H., J. Glodny, F. Lucassen, K. Wemmer, S. Erdmann, R. Handler, and G. Franz (2005), Ordovician metamorphism and plutonism in the Sierra de Quilmes metamorphic complex: Implications for the tectonic

- setting of the northern Sierras Pampeanas (NW Argentina), *Lithos*, 83(1–2), 143–181.
- Carrapa, B., and P. G. DeCelles (2008), Eocene exhumation and basin development in the Puna of northwestern Argentina, *Tectonics*, 27, TC1015, doi:10.1029/2007TC002127.
- Carrera, N., J. A. Munoz, F. Sabat, R. Mon, and E. Roca (2006), The role of inversion tectonics in the structure of the Cordillera Oriental (NW Argentinean Andes), *J. Struct. Geol.*, 28(11), 1921–1932.
- Coira, B., J. Davidson, C. Mpodozis, and V. Ramos (1982), Tectonic and magmatic evolution of the Andes of northern Argentina and Chile, *Earth Sci. Rev.*, 18(3–4), 303–332.
- Coney, P. J., and C. A. Evenchick (1994), Consolidation of the American Cordilleras, *J. South Am. Earth Sci.*, 7(3/4), 241–262.
- Coutand, I., P. R. Cobbold, M. de Urreiztieta, P. Gautier, A. Chauvin, D. Gapais, E. A. Rossello, and O. Lopez-Gamundi (2001), Style and history of Andean deformation, Puna plateau, northwestern Argentina, *Tectonics*, 20(2), 210–234.
- Cristallini, E., A. H. Cominquez, and V. A. Ramos (1997), Deep structure of the Metan-Guachipas region: Tectonic inversion in Northwestern Argentina, *J. South Am. Earth Sci.*, 10(5–6), 403–421.
- Dahlquist, J. A., R. J. Pankhurst, C. W. Rapela, C. Galindo, P. Alasino, C. M. Fanning, J. Saavedra, and E. Baldo (2008), New SHRIMP U-Pb data from the Famatina Complex: Constraining Early Mid Ordovician Famatinian magmatism in the Sierras Pampeanas, Argentina, *Geol. Acta*, 6(4), 319–333.
- Dahlstrom, C. D. A. (1969), Balanced cross sections, *Can. J. Earth Sci.*, 6, 743–757.
- DeCelles, P. G., M. N. Ducea, P. Kapp, and G. Zandt (2009), Cyclicity in Cordilleran orogenic systems, *Nat. Geosci.*, 2(4), 251–257.
- Deeken, A., E. R. Sobel, I. Coutand, M. Haschke, U. Riller, and M. R. Strecker (2006), Development of the southern Eastern Cordillera, NW Argentina, constrained by apatite fission track thermochronology: From early Cretaceous extension to middle Miocene shortening, *Tectonics*, 25, TC6003, doi:10.1029/2005TC001894.
- Dickinson, W. R., and G. E. Gehrels (2009), Use of U-Pb ages of detrital zircons to infer maximum depositional ages of strata: A test against a Colorado Plateau Mesozoic database, *Earth Planet. Sci. Lett.*, 288(1–2), 115–125, doi:10.1016/j.epsl.2009.09.013.
- Ducea, M. N., J. E. Otamendi, G. Bergantz, K. M. Stair, V. A. Valencia, and G. E. Gehrels (2010), Timing constraints on building an intermediate plutonic arc crustal section: U-Pb zircon geochronology of the Sierra Valle Fértil-La Huerta, Famatinian arc, Argentina, *Tectonics*, 29, TC4002, doi:10.1029/2009TC002615.
- Duebendorfer, E. M., and K. L. Meyer (2002), Penetrative strain at shallow crustal levels: The role of pressure solution in accommodating regional shortening strain, Ventura basin, western Transverse Ranges, California, in *Contributions to Crustal Evolution of the Southwestern United States*, edited by A. Barth, *Spec. Pap. Geol. Soc. Am.*, 365, 295–314.
- Egenhoff, S. (2007), Life and death of a Cambrian–Ordovician basin: An Andean three-act play featuring Gondwana and the Arequipa-Antofalla-Terrane, in *The Evolution of the Rheic Ocean: From Avalonian-Cadomian Active Margin to Alleghenian-Variscan Collision*, edited by U. Linnemann et al., *Spec. Pap. Geol. Soc. Am.*, 423, 511–524.
- Erslev, E. A. (1991), Trishear fault-propagation folding, *Geology*, 19(6), 617–620.
- Galliski, M. A. (1983), Distrito minero El Quemado, departamentos La Poma y Cachi, provincia de Salta, *Asoc. Geol. Argent. Rev.*, 38(2), 209–224.
- Gehrels, G. E., V. A. Valencia, and J. Ruiz (2008), Enhanced precision, accuracy, efficiency, and spatial resolution of U-Pb ages by laser ablation–multicollector–inductively coupled plasma–mass spectrometry, *Geochem. Geophys. Geosyst.*, 9, Q03017, doi:10.1029/2007GC001805.
- Grier, M. E., J. A. Salfity, and R. W. Allmendinger (1991), Andean reactivation of the Cretaceous Salta rift, northwestern Argentina, *J. South Am. Earth Sci.*, 4(4), 351–372.
- Hongn, F., and R. Seggiaro (2001), Hoja Geológica 2566-III, Cachi, Provincias de Salta y Catamarca, *Bol. 248*, Inst. de Geol. y Recursos Miner., Serv. Geol. Miner. Argent., Buenos Aires.
- Hongn, F., C. del Papa, J. Powell, I. Petrinovic, R. Mon, and V. Deraco (2007), Middle Eocene deformation and sedimentation in the Puna-Eastern Cordillera transition (23°–26°S): Control by preexisting heterogeneities on the pattern of initial Andean shortening, *Geology*, 35(3), 271–274, doi:10.1130/G23189A.1.
- Hongn, F. D., J. M. Tubia, A. Aranguren, N. Vegas, R. Mon, and G. R. Dunning (2010), Magmatism coeval with lower Paleozoic shelf basins in NW-Argentina (Tastil batholith): Constraints on current stratigraphic and tectonic interpretations, *J. South Am. Earth Sci.*, 29(2), 289–305, doi:10.1016/j.jsames.2009.07.008.
- Isacks, B. L. (1988), Uplift of the central Andean plateau and bending of the Bolivian Orocline, *J. Geophys. Res.*, 93(B4), 3211–3231.
- Ježek, P., A. P. Willner, F. G. Aceñolaza, and H. Miller (1985), The Puncovicana trough - a large basin of Late Precambrian to Early Cambrian age on the Pacific edge of the Brazilian shield, *Geol. Rundsch.*, 74(3), 573–584.
- Kay, S. M., B. Coira, and J. Viramonte (1994), Young mafic back arc volcanic-rocks as indicators of continental lithospheric delamination beneath the Argentine Puna plateau, central Andes, *J. Geophys. Res.*, 99(B12), 24,323–24,339.
- Kley, J., and C. R. Monaldi (1998), Tectonic shortening and crustal thickness in the Central Andes: How good is the correlation?, *Geology*, 26(8), 723–726.
- Kley, J., and C. R. Monaldi (2002), Tectonic inversion in the Santa Barbara System of the central Andean foreland thrust belt, northwestern Argentina, *Tectonics*, 21(6), 1061, doi:10.1029/2002TC902003.
- Kley, J., C. R. Monaldi, and J. A. Salfity (1999), Along-strike segmentation of the Andean foreland: Causes and consequences, *Tectonophysics*, 301(1–2), 75–94.
- Lucassen, F., R. Becchio, H. Wilke, G. Franz, M. Thirlwall, J. Viramonte, and K. Wemmer (2000), Proterozoic-Paleozoic development of the basement of the Central Andes (18–26°S) - a mobile belt of the South American craton, *J. South Am. Earth Sci.*, 13(8), 697–715.
- Ludwig, K. R. (2001), *Isoplot/Ex*, rev. 2.49, *Spec. Publ. 1a*, Berkeley Geochronol. Cent., Berkeley, Calif.
- Marrett, R. A., R. W. Allmendinger, R. N. Alonso, and R. E. Drake (1994), Late Cenozoic tectonic evolution of the Puna Plateau and adjacent foreland, northwestern Argentine Andes, *J. South Am. Earth Sci.*, 7(2), 179–207.
- Masaferro, J. L., M. Bulnes, J. Poblet, and N. Casson (2003), Kinematic evolution and fracture prediction of the Valle Morado structure inferred from 3-D seismic data, Salta Province, northwest Argentina, *AAPG Bull.*, 87(7), 1083–1104.
- McQuarrie, N. (2002), The kinematic history of the central Andean fold-thrust belt, Bolivia: Implications for building a high plateau, *Geol. Soc. Am. Bull.*, 114(8), 950–963.
- Méndez, V., F. E. Nullo, and J. Otamendi (2006), Geoquímica de las Formaciones Puncovicana y Cachi- Sierra de Cachi, Salta, *Asoc. Geol. Argent. Rev.*, 61(2), 256–268.
- Mitra, G. (1994), Strain variation in thrust sheets across the sevier fold-and-thrust belt (Idaho-Utah-Wyoming): Implications for section restoration and wedge taper evolution, *J. Struct. Geol.*, 16(4), 585–602.
- Monaldi, C. R., J. A. Salfity, and J. Kley (2008), Preserved extensional structures in an inverted Cretaceous rift basin, northwestern Argentina: Outcrop examples and implications for fault reactivation, *Tectonics*, 27, TC1011, doi:10.1029/2006TC001993.
- Ogg, J. G., G. Ogg, and F. M. Gradstein (2008), *Concise Geologic Time Scale*, Cambridge Univ. Press, Cambridge, U. K.
- Omarini, R. H., R. J. Sureda, H. J. Gotze, A. Seilacher, and F. Pfluger (1999), Puncovicana folded belt in northwestern Argentina: Testimony of Late Proterozoic Rodinia fragmentation and pre-Gondwana collisional episodes, *Int. J. Earth Sci.*, 88(1), 76–97.
- Oncken, O., D. Hindle, J. Kley, K. Elger, P. Viktor, and K. Schemmann (2006), Deformation of the central Andean upper-plate system: Facts, fiction, and constraints for plateau models, in *Deformation Processes of the Andes*, vol. 1, edited by O. Oncken et al., pp. 3–28, Springer, Berlin.
- Otamendi, J. E., A. M. Tibaldi, G. I. Vujovich, and G. A. Viñao (2008), Metamorphic evolution of migmatites from the deep Famatinian arc crust exposed in Sierras Valle Fértil-La Huerta, San Juan, Argentina, *J. South Am. Earth Sci.*, 25(3), 313–335.
- Otamendi, J. E., L. Pinotti, M. A. S. Basei, and A. Tibaldi (2010), Evaluation of petrogenetic models for intermediate and silicic plutonic rocks from the Sierra de Valle Fértil-La Huerta: Petrologic constraints on the origin of igneous rocks in the Ordovician Famatinian-Puna paleoarc, *J. South Am. Earth Sci.*, 30, 29–45.
- Pardo-Casas, F., and P. Molnar (1987), Relative motion of the Nazca (Farallon) and South American plates since Late Cretaceous time, *Tectonics*, 6(3), 233–248.
- Piñán-Llamas, A., and C. Simpson (2006), Deformation of Gondwana margin turbidites during the Pampean orogeny, north-central Argentina, *Geol. Soc. Am. Bull.*, 118(9/10), 1270–1279.
- Ramos, V. A. (2009), Anatomy and global context of the Andes: Main geologic features and the Andean orogenic cycle, in *Backbone of the Americas: Shallow Subduction, Plateau Uplift, and Ridge and Terrane Collision*, edited by S. M. Kay, V. A. Ramos, and W. R. Dickinson, *Mem. Geol. Soc. Am.*, 204, 31–65.
- Rapela, C. W., R. J. Pankhurst, C. Casquet, E. Baldo, J. Saavedra, and C. Galindo (1998), Early evolution of the Proto-Andean margin of South America, *Geology*, 26(8), 707–710.

- Reiners, P. W. (2005), Zircon (U-Th)/He Thermochronometry, in *Thermochronology*, edited by P. W. Reiners and T. A. Ehlers, *Rev. Mineral. Geochem.*, vol. 58, pp. 151–176, Mineral. Soc. of Am., Washington, D. C.
- Reiners, P. W., and M. T. Brandon (2006), Using thermochronology to understand orogenic erosion, *Annu. Rev. Earth Planet. Sci.*, 34, 419–466.
- Reiners, P. W., S. N. Thomson, D. McPhillips, R. A. Donelick, and J. J. Roering (2007), Wildfire thermochronology and the fate and transport of apatite in hillslope and fluvial environments, *J. Geophys. Res.*, 112, F04001, doi:10.1029/2007JF000759.
- Reiners, P. W., A. Vernon, M. Zattin, G. Gehrels, P. DeCelles, S. N. Thomson, J. Quade, D. Pearson, K. Murray, and W. Cavazza (2010), Detrital thermochronology and growth of the central Andes, *Geol. Soc. Am. Abstr. Programs*, 42(5), 53.
- Reynolds, J. H., C. I. Galli, R. M. Hernandez, B. D. Idleman, J. M. Kotila, R. V. Hilliard, and C. W. Naeser (2000), Middle Miocene tectonic development of the Transition Zone, Salta Province, northwest Argentina: Magnetic stratigraphy from the Metan Subgroup, Sierra de Gonzalez, *Geol. Soc. Am. Bull.*, 112(11), 1736–1751.
- Salfity, J. A., and R. A. Marquillas (1994), Tectonic and sedimentary evolution of the Cretaceous-Eocene Salta Group basin, Argentina, in *Cretaceous Tectonics of the Andes*, edited by J. A. Salfity, pp. 266–315, Vieweg, Braunschweig, Germany.
- Salfity, J. A., and C. R. Monaldi (2006), Hoja Geológica 2566-IV, Metán, Provincia de Salta, *Bol. 319*, Serv. Geol. Min. Argentino, Buenos Aires.
- Schoenbohm, L. M., and M. R. Strecker (2009), Normal faulting along the southern margin of the Puna Plateau, northwest Argentina, *Tectonics*, 28, TC5008, doi:10.1029/2008TC002341.
- Schurr, B., A. Rietbrock, G. Asch, R. Kind, and O. Oncken (2006), Evidence for lithospheric detachment in the central Andes from local earthquake tomography, *Tectonophysics*, 415(1–4), 203–223.
- Schwartz, J. J., L. P. Gromet, and R. Miro (2008), Timing and duration of the calc-alkaline arc of the Pampean Orogeny: Implications for the late Neoproterozoic to Cambrian evolution of western Gondwana, *J. Geol.*, 116(1), 39–61.
- Sheffels, B. M. (1990), Lower bound on the amount of crustal shortening in the central Bolivian Andes, *Geology*, 18(9), 812–815.
- Stacey, J. S., and J. D. Kramers (1975), Approximation of terrestrial lead isotope evolution by a 2-stage model, *Earth Planet. Sci. Lett.*, 26(2), 207–221.
- Strecker, M. R., R. N. Alonso, B. Bookhagen, B. Carrapa, G. E. Hilley, E. R. Sobel, and M. H. Trauth (2007), Tectonics and climate of the southern central Andes, *Annu. Rev. Earth Planet. Sci.*, 35, 747–787, doi:10.1146/Annurev.Earth.35.031306.140158.
- Trauth, M. H., R. A. Alonso, K. R. Haselton, R. L. Hermanns, and M. R. Strecker (2000), Climate change and mass movements in the NW Argentine Andes, *Earth Planet. Sci. Lett.*, 179(2), 243–256.
- Turner, J. C. M. (1960), Estratigrafía de la Sierra de Santa Victoria y adyacencias, *Bol. Acad. Nac. Cienc. Córdoba*, 41, 163–196.
- Weil, A. B., A. Yonkee, and A. Sussman (2010), Reconstructing the kinematic evolution of curved mountain belts: A paleomagnetic study of Triassic red beds from the Wyoming salient, Sevier thrust belt, USA, *Geol. Soc. Am. Bull.*, 122(1–2), 3–23, doi:10.1130/B26483.1.
- Williams, G., and T. Chapman (1983), Strains developed in the hanging walls of thrusts due to their slip/propagation rate: A dislocation model, *J. Struct. Geol.*, 5(6), 563–571.
- Wölbern, I., B. Heit, X. Yuan, G. Asch, R. Kind, J. Viramonte, S. Tawackoli, and H. Wilke (2009), Receiver function images from the Moho and the slab beneath the Altiplano and Puna plateaus in the Central Andes, *Geophys. J. Int.*, 177(1), 296–308, doi:10.1111/J.1365-246X.2008.04075.X.
- Yonkee, A., and A. B. Weil (2010), Reconstructing the kinematic evolution of curved mountain belts: Internal strain patterns in the Wyoming salient, Sevier thrust belt, USA, *Geol. Soc. Am. Bull.*, 122(1–2), 24–49, doi:10.1130/B26484.1.
- Yuan, X., S. V. Sobolev, and R. Kind (2002), Moho topography in the central Andes and its geodynamic implications, *Earth Planet. Sci. Lett.*, 199(3–4), 389–402.